Inorganic Chemistry

Article

pubs.acs.org/IC

Dinuclear Seven-Coordinate Mn(II) Complexes: Effect of Manganese(II)-Hydroxo Species on Water Exchange and Superoxide Dismutase Activity

Dominik Lieb, Felix C. Friedel, Mirza Yawer, Achim Zahl, Marat M. Khusniyarov, Frank W. Heinemann, and Ivana Ivanović-Burmazović*

Department of Chemistry and Pharmacy, University of Erlangen-Nürnberg, Egerlandstr. 1, 91058 Erlangen, Germany

Supporting Information

ABSTRACT: Two dinuclear seven-coordinate manganese(II) complexes containing two pentaazamacrocyclic subunits, with imine or amine functionalities, respectively, have been synthesized and characterized in the solid state as well as in aqueous solutions of different pH, by performing X-ray structure analyses, SQUID, potentiometric, electron spray ionization-mass spectrometry (ESI-MS), electrochemical, and ^{17}O NMR water exchange measurements (varying temperature and pressure), and by determination of SOD activity. The two manganese(II) centers within the dinuclear structures behave independently from each other and similarly to the manganese centers in the corresponding mononuclear complexes. However, the dinuclear amine complex possesses increased complex stability and acidity of the coordinated water molecules (pK_{a2} = 8.92) in comparison to the corresponding mononuclear analogue. This allowed us to observe a stable *trans*-aqua-hydroxo-Mn(II) species in an aqueous solution and to study for the first time the *trans*-effect of the hydroxo group on the water lability on any divalent metal center in general. The observed *trans*-labilizing effect of the hydroxo ligand is much smaller than in the case of aqua-hydroxo-M(III) trivalent metal species. Whether this is a general property of *trans*-aqua-hydroxo-M(II) species, or if it is specific for Mn(II) and/or to the seven-coordinate structures, remains to be seen and motivates future studies. In addition, an influence of the hydroxo ligand on the SOD activity of manganese(II) complexes could be evaluated for the first time as well. Compared with the mononuclear analogue, which is not able to form stable hydroxo species, our pH dependent studies on the SOD activity of the dinuclear amine complex have indicated that the hydroxo ligand may promote protonation and release of the product H_2O_2, especially in solutions of higher pH values, by increasing its pK_a value.

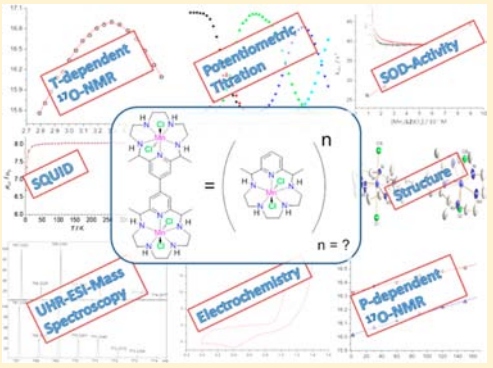

INTRODUCTION

The redox rich chemistry of manganese centers is usually related to their function in metalloenzymes[1] and enzyme mimetics,[2] their application in redox catalysis,[3] as well as application as magnetic materials[4] and new battery technologies.[5] In the biomedical area manganese is associated with oxidative stress protection,[6] imaging applications,[7,8] and supplementation of biomaterials,[9] as well as with neurotoxicity.[10] Whereas higher manganese oxidation states are involved in the processes of water oxidation and hydrogen peroxide disproportionation by the oxygen evolving complex (OEP) and catalase,[11] respectively, within the catalytic cycle of superoxide dismutase (SOD) the metal center alternates between the Mn(II) and Mn(III) states.[12] The Mn(II) chemistry also plays a role in the development of medical diagnostic tools of supposedly lower toxicity than commonly used gadolinium(III) probes. High-spin Mn(II) can efficiently enhance the relaxation rates of water protons (due to its large spin number, fast water exchange rates and long electronic relaxation times), which is a basic principle of action of contrast agents for magnetic resonance imaging (MRI).[8] The existence of a labile, i.e., easily accessible coordination site is an important prerequisite for the involvement of an inner-sphere electron transfer mechanism in the activation of small molecules by metal centers, as in the case of SOD catalysis.[13] The presence of labile inner-sphere aqua ligands is also important for high contrast agent efficiency of manganese(II) complexes, and the higher the inner-sphere hydration number (q) is, the stronger the relaxation enhancement is.[14] Thus, aqua-Mn(II) complexes, especially those with more than one inner-sphere water molecule, are interesting structural motifs, both for design of efficient SOD mimetics and MRI contrast agents. Besides structural and stability requirements, solution properties of these complexes are crucial for their bioapplication and deserve special attention. In particular, lability of coordinated water molecules, reflected in rates of water exchange on Mn(II), is an important parameter that should be high enough to not limit catalysis and reactivity, respectively. Due to the fact that Mn(II) is quite labile and therefore offers fast solvent exchange rates, it

Received: August 7, 2012
Published: December 20, 2012

is a challenge to design a complex that will also meet other requirements, i.e., to have a maximum number of labile inner-sphere water molecules and at the same time to be thermodynamically stable under physiological conditions.[2]

One possible approach, yet not well exploited, is to utilize dinuclear, or in general polynuclear, structural frameworks for design of more stable manganese(II) complexes with a potential biomedical application. Such a design platform might bring other interesting features as well. In comparison to mononuclear complexes, bigger and more rigid dinuclear structures result in slower rotational dynamics that enhances relaxivity. Furthermore, proximal chelation of two (or more) manganese(II) centers causes a local concentration of paramagnetic centers and may increase overall positive charge and the number of inner-sphere aqua ligands within a molecular entity. Increased hydrophobicity or higher positive charge might influence distribution of a complex within subcellular compartments and increase its accumulation in mitochondria,[15,16] which would be a favorable property for a potential SOD mimetic. In general, an SOD activity or electronic relaxivity comparable with that of a mononuclear complex of similar structure could be achieved with solutions of lower osmotic pressure by using dinuclear (or polynuclear) complexes.

From a fundamental point of view, manganese dinuclear structures are still a challenging research area. It is known that electronic communication between manganese centers within dinuclear structures has an influence on their redox properties. However, what influence a close proximity of the second manganese center has on other properties of dinuclear Mn(II) complexes in aqueous solutions (i.e., stability, acid−base equilibria, lability of aqua ligands, etc.) is less known. Only in the case of the dinuclear $[Mn_2(ENOTA)(H_2O)_2]$ complex (Chart 1), where each manganese(II) center has one inner-sphere water bound, detailed investigations in solution were performed, including water exchange studies.[17] However, the solution behavior of a Mn(II) dinuclear complex with more than one inner-sphere water molecule is not reported yet. This limits our understanding of how variation/binding of other ligands influences kinetics of water exchange on Mn(II), which is an important determinant concerning a compound's biomedical application. On one hand, such knowledge allows us to predict the effects of target biomolecules[18] as well as other small species inevitably present under physiological conditions[19] on relaxivity/SOD activity of a dinuclear structure of interest. On the other hand, this enables rational tuning and optimization of water lability to create high relaxivity contrast agents or efficient SOD mimetics, respectively, based on the dinuclear framework.

Chart 1. Ligand Structures of Manganese Complexes Studied or Discussed in This Work

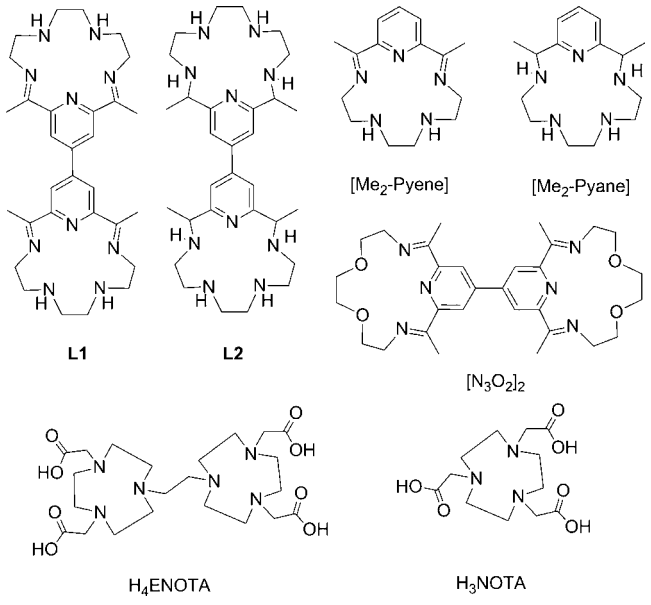

One of the basic effects known to significantly control the substitution behavior of metal complexes in aqueous solutions is the *trans*-labilizing effect of a hydroxo group.[20] Although it is well established in the chemistry of trivalent aqua-hydroxo-M(III) metal species, where it can increase a water lability up to 4 orders of magnitude,[21] to our best knowledge there is no literature report on a *trans*-labilizing effect of hydroxo ligands on the water molecule coordinated to any divalent metal ion in general. The only water exchange rate constant, k_{ex}, in the case of M(II) aqua-hydroxo complexes that is known in the literature is the exchange rate estimated for the water molecules in the *cis* positions with respect to the hydroxo group in *fac*-$[Ru(CO)_3(OH)(H_2O)_2]^+$.[22] Stable aqua-hydroxo-M(II) species are not easily accessible in aqueous solutions due to the lower acidity of the aqua-M(II) ions in comparison to aqua-M(III), with their tendency to oxidize and to dimerize/polymerize.[23] Therefore, an interesting paradigm is to probe dinuclear structural frameworks as a tool to tune acidity of the aqua-M(II) ion and to create an aqua-hydroxo-Mn(II) species, preferably more stable than a corresponding mononuclear analogue. By way of comparison the $[Mn_2(ENOTA)(H_2O)_2]$ dinuclear complex exhibits a lower stability as compared to that of the mononuclear analogue [Mn(NOTA)] (Chart 1).[17]

In general, *trans*-labilization of an aqua ligand affects the solution behavior of metal complexes, e.g., by enhancing the reactivity of the metal center.[24] Thus, it would be also interesting to probe whether formation of *trans*-HO-Mn(II)-OH_2 species have an influence on the SOD activity of manganese centers. Even more, dinuclear Mn-SOD mimetics have not been investigated so far, which is an additional motivation to pursue studies on manganese(II) complex with two active centers.

In order to shed light on the above-mentioned aspects of manganese(II) solution chemistry, we have synthesized manganese(II) dinuclear complexes with more than one aqua ligand per metal center and with a potential SOD activity. To achieve the desired structure−reactivity properties we have utilized pentaazamacrocyclic ligand scaffolds (**L1** and **L2** in Chart 1), known to promote SOD activity and stability of the Mn(II) complexes, respectively, in combination with a 2,2′,6,6′-tetraacetyl-4,4′-bipyridine building block, originally applied for the design of novel materials with characteristics of molecule-based magnets.[4] The mononuclear analogues, with the Me_2-Pyene and Me_2-Pyane ligands (Chart 1), were studied in detail regarding the mechanism of their SOD catalysis, water exchange kinetics, and thermodynamic stability,[25,26] which enables a direct comparison of the corresponding reactivity/stability parameters. In the case of the amine structure we were able to demonstrate that the dinuclear framework can offer a useful platform for increased stability of Mn(II) complexes that at the same time possess two water molecules per metal center with an increased acidity, resulting in the generation of uniquely

dx.doi.org/10.1021/ic301714d | Inorg. Chem. 2013, 52, 222−236

Scheme 1. Synthesis of 2,2′,6,6′-Tetraacetyl-4,4′-bipyridine (Abbreviated as Tabpy)

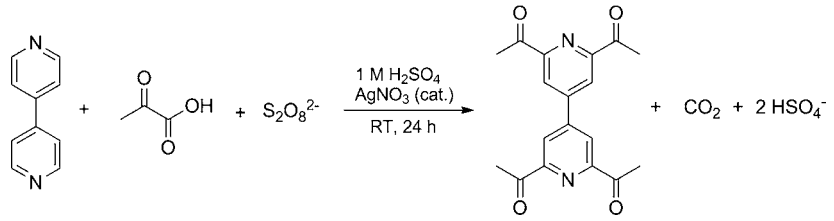

stable aqua-hydroxo-Mn(II) species in the aqueous solution. Therefore, we could examine for the first time the *trans*-effect of the hydroxo group on water exchange in manganese(II) complexes and consequently on its catalytic SOD activity, which is generally a unique study in the chemistry of divalent metal ions.

EXPERIMENTAL SECTION

General. All reactions were performed under an argon atmosphere. Reagents and solvents that were commercially available were purchased from Sigma-Aldrich or Acros Organics, were of *p.a.* (*pro analysi*) grade, and were used without further purification. Only anhydrous solvents (purchased from Sigma Aldrich or Acros Organics) were used for synthesis. Deionized Millipore water was used for all measurements. Carlo Erba elemental analyzers 1106 and 1108 and a Bruker Avance DPX 300 NMR spectrometer were used for elemental and NMR analyses, respectively. IR spectra were recorded as KBr pellets on a Mattson FT-IR 60 AR. Temperature-dependent magnetic susceptibility data were recorded on an MPMS XL Quantum Design SQUID magnetometer in the temperature range 2−300 K. The experimental magnetic susceptibility data were corrected for underlying diamagnetism and temperature-independent paramagnetism (TIP). The program JulX v.1.5 was used to fit experimental data.[27]

Synthesis of 2,2′,6,6′-Tetraacetyl-4,4′-bipyridine (Tabpy) (Scheme 1). Tabpy was obtained using a somewhat modified literature procedure.[28] 4,4′-Bipyridine (5 g, 32.05 mmol), pyruvic acid (19.266 g, 224 mmol), and $AgNO_3$ (0.414 g 2.4 mmol, dissolved in 5 mL of water) were dissolved in 620 mL of a 0.4 M H_2SO_4 solution. Ammonium persulfate (56.832 g, 256 mmol) was carefully added in small portions (strong gas evolution!) and with intense stirring. The mixture was stirred at room temperature overnight, and the resultant white precipitate was filtered off. A 5 mL portion of conc H_2SO_4 was added to the filtrated solution, and the solution was subsequently treated with the same amounts of pyruvic acid, $AgNO_3$, and ammonium persulfate as for the first time (*vide supra*). The mixture was stirred again overnight at room temperature and the precipitate filtered. The collected solids were combined and purified by column chromatography (ethyl acetate/hexane/dichloromethane in a ratio of 10/20/70, R_f = 0.8). The product was obtained as white thin needles (1.35 g, 13%). Anal. Calcd for $C_{18}H_{16}N_2O_4$: C, 66.66; H, 4.97; N, 8.64. Found: C, 66.59; H, 5.01; N 8.60. ^{1}H NMR (400 MHz, $CDCl_3$, 25 °C): δ [ppm] = 2.78 (s, 12H, CH_3), 8.48 (s, 4H, ArH). ^{13}C NMR (100 MHz, $CDCl_3$, 25 °C): δ [ppm] = 25.68, 122.25, 146.69, 153.98, 198.76 . IR (KBr): $\tilde{\nu}$ [cm^{-1}] 3380 (m), 2360 (m), 1589 (s, C═O), 1363 (s), 1302 (m), 1236 (m), 1099 (m).

Synthesis of $[Mn_2(L1)Cl_4]$. Tabpy (1.62 g, 5.0 mmol) was suspended in 100 mL of methanol (MeOH), and $MnCl_2{\cdot}4H_2O$ (1.98 g, 10.05 mmol, dissolved in 20 mL methanol) was added with stirring. The slurry was kept at 60 °C for 30 min after which triethylenetetraamine (3.24 mL, 1.46 g, 10.00 mmol in 25 mL methanol) was slowly added via a dropping funnel. The mixture turned slowly orange and was refluxed for 7 h, after which a deep orange solution was obtained. The solution was concentrated to about 30 mL and left in the refrigerator overnight. The resultant orange precipitate was filtered off, washed with small amounts of ethanol, and dried. $[Mn_2(\mathbf{L1})Cl_4]$ was obtained as a deep orange powder (3.61 g, 80%). Anal. Calcd for $[Mn_2(\mathbf{L1})Cl_4]{\cdot}4\ H_2O{\cdot}MeOH$: C, 41.35; H, 6.27; N, 15.55. Found: C, 40.97, H, 6.16, N, 15.76. IR (KBr): $\tilde{\nu}$ [cm^{-1}] 3392 (m), 2917 (w), 2861 (w), 1646 (s, C═N), 1606 (m), 1458 (m), 1426 (m), 1378 (s), 1273 (m), 1107 (m), 875 (w), 729 (m), 640 (m), 443 (w).

Synthesis of $[Mn_2(L2)Cl_4]$. $[Mn_2(\mathbf{L2})Cl_4]$ was obtained by reduction of $[Mn_2(\mathbf{L1})Cl_4]$ with sodium borohydride similar to the published procedure.[29] $[Mn_2(\mathbf{L1})Cl_4]$ (1.0 g, 1.1 mmol) was dissolved in absolute ethanol (EtOH), and argon was bubbled through the stirring solution for 15 min. Sodium borohydride (0.6 g, 16.0 mmol, 16 equiv) was added in four portions in 15 min time intervals. The mixture was stirred for 1 h at room temperature and then for 8 h at 60 °C. Afterward, the solvent was removed under vacuum, and 30 mL of 1 M LiCl in methanol was added and stirred until all gas evolution stopped. Methanol was removed, and 50 mL of brine was added to the light brown residue. The aqueous solution was extracted 3 times with DCM (dichloromethane) and 3 times with DCM/ethanol (90:10). The combined organic phases were dried over anhydrous $MgSO_4$, and after removal of solvent $[Mn_2(\mathbf{L2})Cl_4]$ was obtained as a deep yellow powder (0.41 g, 40%). Anal. Calcd for $[Mn_2(\mathbf{L2})Cl_4]{\cdot}4H_2O{\cdot}EtOH$: C, 41.66; H, 7.21; N, 15.18. Found: C, 41.79, H, 7.31, N, 15.21. IR (KBr): $\tilde{\nu}$ [cm^{-1}] 3583 (m), 2968 (w), 2921 (m), 2868 (w), 1606 (m), 1549 (m), 1455 (m), 1398 (s), 1321 (m), 1094 (m), 1048 (m), 1008 (w), 968 (m), 879 (w), 819 (m), 599 (w).

X-ray Crystal Structure Determinations for $[Mn_2(L1)Cl_4]$ and $[Mn_2(L2)Cl_4]$. Single crystals suitable for X-ray analysis of $[Mn_2(\mathbf{L1})Cl_4]$ and $[Mn_2(\mathbf{L2})Cl_4]$ were obtained by slow diffusion of Et_2O vapor into a 1 mM methanol solution of the respective complex, standing for several days in the refrigerator. Dark orange crystals were obtained for $[Mn_2(\mathbf{L1})Cl_4]$, and yellow crystals were obtained for $[Mn_2(\mathbf{L2})Cl_4]$. Data were collected on a Bruker Kappa APEX 2 *IμS* Duo diffractometer with MoKα radiation (QUAZAR focusing Montel optics, λ = 0.710 73 Å) at 100 K. Lorentz and polarization corrections as well as semiempirical absorption corrections based on multiple scans were applied to both data sets (*SADABS 2.11*, Bruker AXS, 2009). The structures of both manganese(II) complexes were solved by direct methods and refined using full-matrix least-squares procedures on F^2 (*SHELXTL NT 6.12*, Bruker AXS, 2002). Both complexes crystallized with four molecules of methanol per molecule of complex, and all of the solvent molecules are disordered. In both cases the dinuclear complex molecule is situated on a 2-fold crystallographic rotation axis running through the two Mn(II) atoms and the central atoms N1, N4, C1, and C9. One of the independent chloro atoms in $[Mn_2(\mathbf{L1})Cl_4]$ is disordered. Two alternative sites were refined with occupancies of 63(6)% and 37(6)% for Cl1 and Cl1A, respectively. The ligand is subjected to disorder, with two equally occupied sites being refined for the atoms N6, C15, C16 and N6A, C15A, and C16A. In $[Mn_2(\mathbf{L2})Cl_4]$ both independent chloro atoms are disordered. Two alternative sites were refined with occupancies of 56(10)% and 44(10)% for Cl1 and Cl1A and 71(3)% and 29(3)% for Cl2 and Cl2A, respectively. The ligand is also subjected to disorder; two alternative sites were refined resulting in site occupancy factors of 61(2)% for the atoms N2, N3, C4, C7, C8 and 39(2)% for the atoms N2A, N3A, C4A, C7A, and C8A. DFIX, SIMU, and ISOR restraints were applied in the refinement of the disordered structure parts. All hydrogen atoms were placed in positions of optimized geometry; their isotropic displacement parameters were tied to those of their corresponding carrier atoms by a factor of 1.2 or 1.5.

CCDC 838452 for $[Mn_2(\mathbf{L1})Cl_4]{\cdot}4MeOH$, CCDC-838453 for $[Mn_2(\mathbf{L2})Cl_4]{\cdot}4MeOH$, and CCDC-838583 for tabpy contain the supplementary crystallographic data. These data can be obtained free

dx.doi.org/10.1021/ic301714d | *Inorg. Chem.* 2013, 52, 222−236

of charge from The Cambridge Crystallographic Data Centre via www.ccdc.cam.ac.uk/data_request/cif.

A summary of important crystallographic data, data collection and refinement details is presented in Table 1.

Table 1. Crystallographic Parameters, Data Collection, and Refinement Details for $[Mn_2(L1)Cl_4]\cdot 4MeOH$ and $[Mn_2(L2)Cl_4]\cdot 4MeOH$

	$[Mn_2(\mathbf{L1})Cl_4]\cdot 4MeOH$	$[Mn_2(\mathbf{L2})Cl_4]\cdot 4MeOH$
empirical formula	$C_{34}H_{60}Cl_4Mn_2N_{10}O_4$	$C_{34}H_{68}Cl_4Mn_2N_{10}O_4$
M_r	924.60	932.66
color and shape	prism, dark orange	prism, yellow
cryst syst	monoclinic	monoclinic
space group	$C2/c$	$C2/c$
a (Å)	20.051(4)	19.718(3)
b (Å)	21.294(4)	21.431(3)
c (Å)	10.968(2)	11.333(2)
α (deg)	90	90
β (deg)	113.622(3)	112.073(4)
γ (deg)	90	90
V (Å^3)	4290(2)	4438(2)
Z	4	4
D_{calc} (g cm^{-3})	1.431	1.396
μ (mm^{-1})	0.886	0.857
$F(000)$	1936	1968
T_{min}/T_{max}	0.667/0.746	0.675/0.746
2Θ interval (deg)	$5.7 \le 2\Theta \le 54.2$	$5.4 \le 2\Theta \le 52.8$
reflns collected	18 538	29 816
reflns unique	4726	4540
reflns obsd $[I > 2\sigma(I)]$	3440	3717
refined params	311	318
final R indices $[I > 2\sigma(I)]$	R1 = 0.0578, wR2 = 0.1484	R1 = 0.0547, wR2 = 0.1549
R indices (all data)	R1 = 0.0860, wR2 = 0.1649	R1 = 0.0666, wR2 = 0.1635
GOF on F^2	1.290	1.199
$\Delta\rho_{max/min}$ (e Å^{-3})	1.393/−0.863	0.855/−0.595

Electron-Spray-Ionization (ESI) Mass Spectrometry. High mass accuracy ESI spectra were recorded on an ultrahigh-resolution ESI-time-of-flight MS, a Bruker Daltoniks (Bremen, Germany) maXis. Spectra were obtained in positive-ion mode, with the capillary held at 4000 V. The drying gas flow rate was 7.0 L min^{-1} with a temperature of 180 °C for standard and 4 °C for the cryo-spray measurements at higher pH. The nebulizer gas was at a pressure of 30.5 psi/2 bar. The m/z range detected was from 100 to 2000. A calibration tune mix (Agilent Technologies) was sprayed immediately prior to analysis to ensure a high mass accuracy to assist in the identification of peaks. The flow rate of the solutions was 300 μL/h. The samples were dissolved in aqueous solutions of the corresponding pH values, and the complex concentrations were 1 mM each. Peaks were identified with the aid of the simulated isotopic patterns created within the Bruker DataAnalysis software.

Electrochemistry. Cyclic voltammetry measurements were performed using an Autolab instrument with a PGSTAT 30 potentiostat. A three-electrode arrangement was employed consisting of a gold disk working electrode (A = 0.07 cm^2) (Metrohm), a platinum auxiliary electrode (Metrohm), and a Ag/AgCl, (LiCl 2 M in EtOH) (Metrohm) reference electrode (0.164 V vs NHE at 20 °C), for the measurements in DMSO, or a Ag/AgCl (NaCl 3 M) (Metrohm) reference electrode (0.222 V vs NHE at 20 °C), for measurements in the aqueous solution. The measurements in DMSO were performed in the presence of 0.1 M tetrabutylammonium hexafluorophosphate as the supporting electrolyte, and the measurements in aqueous solutions were performed in 0.05 M buffer solutions at pH 7.0 (PIPES buffer) and at pH 10.0 (CAPS buffer) with additional 0.05 M NaCl as supporting electrolyte. All solutions were degassed with nitrogen (1 min/mL), and during the measurements, the nitrogen atmosphere was maintained. The sample concentration was 1.0 mM for each complex, the scan rates were 100 mV/s, and the experiments were performed at 20 °C.

Potentiometric Titrations. Potentiometric measurements were performed on a METROHM 702 SM Titrino in a jacketed, airtight glass titration cell equipped with a combined pH glass electrode (METROHM), N_2 inlet and outlet, and a graduated 10 mL microburet (METROHM). The electrode was filled with NaCl instead of KCl to prevent precipitation of $KClO_4$ and was calibrated using three different commercially available standard buffer solutions of pH 4.0, 7.0, and 10.0. A carbonate-free 0.05 M sodium hydroxide or perchloric acid solution was prepared with nitrogen-saturated deionized Millipore water. The NaOH solution was standardized by titrations with a 0.05 M potassium hydrogen phthalate solution and then used for standardization of the perchloric acid solution. Gran's method[30] was used to measure carbonate in the sodium hydroxide standard solution (carbonate content 0.10%). All solutions were adjusted to an ionic strength of 0.1 M with $NaClO_4$ prior to the titrations. The temperature was maintained by circulating thermostatted water through the outer jacket of the cell. All measurements were carried out while a constant atmosphere of nitrogen was maintained above the solution. The concentration of complexes was 1.0 mM for each titration. Species distribution calculations and determination of the corresponding protonation equilibrium and stability constants were performed using the computer program TITFIT.[31]

^{17}O NMR Measurements. 10%-Enriched ^{17}O-labeled water (D-Chem Ltd. Tel Aviv, Israel) was used for the ^{17}O NMR water-exchange measurements. The complex samples were prepared by combining weighed amounts of complex in an appropriate buffer solution, i.e., a 1,4-piperazinediethanesulfonic acid buffer (PIPES) for measurement at pH 7.0/7.5 and a *N*-cyclohexyl-3-aminopropanesulfonic acid buffer (CAPS) at pH 9.3, 10.0, and 11.0. These buffers were chosen because they do not interfere with the ^{17}O NMR dependent measurements as their pK_a values are neither pressure nor temperature dependent.[32] The resulting solution was transferred to the NMR tube under an argon atmosphere. The pH was determined in a NMR tube using a micro pH meter, Innovative Instruments, Inc. The concentrations of the complexes were 10, 15, or 20 mM in 0.2 M of the respective buffer solutions. Variable-temperature/pressure Fourier-transform ^{17}O NMR spectra were recorded at a frequency of 54.24 MHz and at a magnetic induction of 9.4 T on a Bruker Advance DRX 400WB spectrometer equipped with a superconducting BC-94/89 magnet system. The temperature dependence of the ^{17}O-line broadening was studied over the temperature range from 274.2 to 338.2 K, for $[Mn_2(\mathbf{L1})Cl_4]$, and in the range from 274.2 to 358.2 K, for compound $[Mn_2(\mathbf{L2})Cl_4]$. A homemade high-pressure probe described in the literature[33] was used for the variable-pressure experiments, which were conducted at the specified temperature and at ambient, 2, 30, 60, 90, 120, and 150 MPa pressures. A standard 5 mm NMR tube cut to a length of 50 mm was used for the sample solutions. The pressure was transmitted by a movable macor piston, and the temperature was controlled as described elsewhere.[33] For all measurements a reference spectra from the pure solvent without complex (i.e., blank buffer at pH 7.0, 7.5, 9.3, 10.0, or 11.0) was first recorded to subtract the influence of the solvent on the water exchange.

Direct Determination of SOD Activity via Stopped-Flow Measurements. The SOD activity of the complexes was determined by using direct rapid-scan UV−vis detection of superoxide decomposition in aqueous media and global analysis of the entire time-resolved spectra. This method requires a double mixer stopped-flow system equipped with a high-density mixer, for efficient mixing of aqueous buffer solutions containing the investigated complexes, with a DMSO solution of KO_2 (in a 10:1 ratio). This system is combined with a fast diode array detector (0.5 ms integration time) and a laser driven light source. The exact experimental method used for determination of the SOD activity of the two novel dinuclear Mn(II)

dx.doi.org/10.1021/ic301714d | *Inorg. Chem.* 2013, 52, 222−236

Scheme 2. Synthetic Route for the Dinuclear Complexes $[Mn_2(L1)Cl_4]$ and $[Mn_2(L2)Cl_4]$

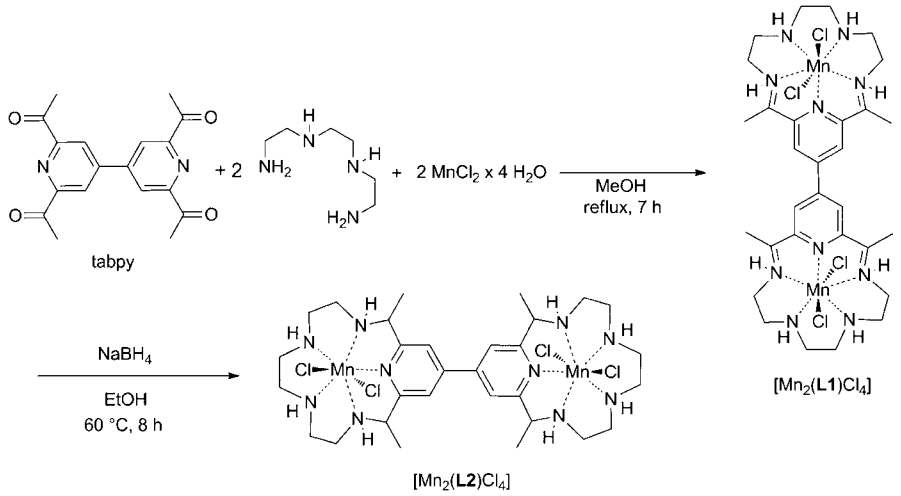

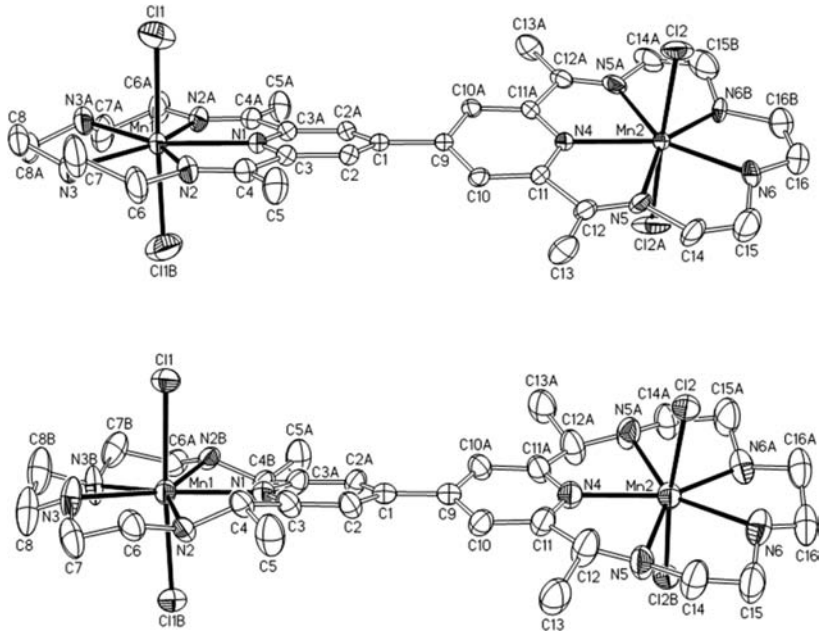

Figure 1. Thermal ellipsoid representation of the molecular structure of $[Mn_2(L1)Cl_4]$ in crystals of $[Mn_2(L1)Cl_4]\cdot 4MeOH$ (top) and $[Mn_2(L2)Cl_4]$ in crystals of $[Mn_2(L2)Cl_4]\cdot 4MeOH$ (bottom) with the applied numbering scheme (50% probability ellipsoids; hydrogen atoms, disorder, and cocrystallized solvent molecules omitted for clarity).

complexes $[Mn_2(L1)Cl_4]$ and $[Mn_2(L2)Cl_4]$ is published elsewhere.[19] In general the measurements were carried out in 60 mM 4-(2-hydroxyethyl)-1-piperazineethanesulfonic acid buffer (HEPES) at pH 7.4 or 8.1, respectively, or 60 mM CAPS buffer at pH 10.0, prepared with Millipore water and treated with chelex 100 chelating resin for at least 24 h to catch trace metal ions. The complex was dissolved in a buffer solution, previously treated with chelex 100. Truly catalytic conditions were used with a high excess of superoxide (ca. 2.0×10^{-4} M)[34] over the complexes, which were used in concentrations of 1.13, 2.25, 4.50, and 9.0×10^{-7} M.

RESULTS AND DISCUSSION

Syntheses and Molecular and Crystal Structures. Synthesis of 2,2′,6,6′-tetraacetyl-4,4′-bipyridine (tabpy) has been reported previously, where Fe(II) was used as an initiator in a radical-based synthesis.[35] However, purification of the product is very difficult due to a number of side products obtained by that synthetic procedure. Therefore, we have used a different method to synthesize tabpy, similar to an already known procedure,[28] where silver(I) was used as a radical initiator instead of iron(II) (Scheme 1). The yield obtained is somewhat higher than that reported in the literature,[35] and the advantage of the applied method is an easier work up and product purification. Crystal structure and crystallographic data for (tabpy) are shown in Supporting Information (Figure S1 and Table S1).

$[Mn_2(L1)Cl_4]$ was synthesized in absolute MeOH under an argon atmosphere via a template method[36] from manganese(II) chloride, triethylenetetramine, and tabpy. The reduced complex, $[Mn_2(L2)Cl_4]$, was obtained by treatment of $[Mn_2(L1)Cl_4]$ with sodium borohydride in absolute EtOH under an argon atmosphere. The synthesis, molecular structure, and selected bond lengths for both complexes are presented in Scheme 2, Figure 1, and Table 2, respectively.

dx.doi.org/10.1021/ic301714d | Inorg. Chem. 2013, 52, 222−236

Table 2. Selected Bond Distances (Å) for Molecular Structures of $[Mn_2(L1)Cl_4]\cdot 4MeOH$ and $[Mn_2(L2)Cl_4]\cdot 4MeOH$[a]

	$[Mn_2(L1)Cl_4]$	$[Mn_2(L2)Cl_4]$
Mn1−N1	2.256(4)	2.264(4)
Mn1−N2	2.288(4)	2.328(8)
Mn1−N2A/B	2.288(4)	2.371(11)
Mn1−N3	2.299(3)	2.32(2)
Mn1−N3A/B	2.299(3)	2.32(2)
Mn1−Cl1	2.543(7)	2.612(18)
Mn1−Cl1B	2.576(8)	2.539(15)
Mn2−N4	2.253(4)	2.273(4)
Mn2−N5	2.290(3)	2.322(4)
Mn2−N5A	2.290(3)	2.322(4)
Mn2−N6	2.252(9)	2.310(3)
Mn2−N6A	2.252(9)	2.310(3)
Mn2−Cl2	2.5662(12)	2.593(3)
Mn2−Cl2A	2.5663(12)	2.579(9)

[a]Symmetry transformations used to generate equivalent atoms: $-x + 1, y, -z + {}^1/_2$.

In the crystal structures of $[Mn_2(L1)Cl_4]$ and $[Mn_2(L2)Cl_4]$, the dinuclear complex molecules are situated on 2-fold crystallographic rotation axes running through the two manganese atoms with the central atoms N2, N4, C2, and C9 thus enforcing C_2 molecular symmetry. In both complexes the two manganese atoms are seven-coordinate in a pentagonal bipyramidal environment as is also the case for the mononuclear analogues[37,38] and other manganese(II) complexes containing pentadentate macrocyclic ligands in the literature.[4,39] The five nitrogen atoms of the macrocycle adopt the equatorial positions, and the two chlorido ligands occupy the axial positions resulting in a Cl−Mn−Cl angle close to 180° with the biggest deviation from linearity of 6.3° (Cl2−Mn2−Cl2B) observed in $[Mn_2(L2)Cl_4]$ (see Table 3). The Mn−Cl distances are similar for both compounds and lie in a range between 2.54 and 2.61 Å. The macrocyclic units of the imine complex $[Mn_2(L1)Cl_4]$ are nearly planar with maximum deviations from the MnN_5 least-squares plane of 0.107(4) Å for N3 and N3A in the first plane ($Mn1N_5$) and 0.247(7) Å for N6 and N6A in the second plane ($Mn2N_5$). The maximum deviations from the corresponding planes in the saturated amine complex $[Mn_2(L2)Cl_4]$ are 0.26(2) Å for N3 and N3A in the first plane ($Mn1N_5$) and 0.216(4) Å for N6 and N6A in the second plane ($Mn2N_5$). Due to the molecule's position on a 2-fold axis, in the case of both complexes, the two Mn(II) atoms are to be found exactly within the MnN_5 least-squares plane. As it is observed for their mononuclear analogues,[37] the average Mn−N distances are shorter in the imine complex $[Mn_2(L1)Cl_4]$ as compared to the amine complex $[Mn_2(L2)Cl_4]$. A comparison of the Mn−N distances of mononuclear [Mn(Me$_2$-Pyene)] (2.254(2)−2.316(2) Å)[37] with dimeric $[Mn_2(L1)Cl_4]$ (2.253(4)−2.299(3) Å) yields very similar values indicating no significant differences in the Mn−N bond lengths between the two complexes. The same trend is found for [Mn(Me$_2$-Pyane)] with Mn−N distances ranging from 2.278(3) to 2.352(3) Å and its corresponding dinuclear complex $[Mn_2(L2)Cl_4]$ with Mn−N bond lengths lying between 2.264(4) and 2.371(11) Å. The dihedral angle between the two planes of the pyridine rings of $[Mn_2(L1)Cl_4]$ and $[Mn_2(L2)Cl_4]$ amount to 28.4(2)° and 19.8(2)°, respectively, which is much smaller than the value of 41° reported for $[Mn(N_3O_2)]_2$ (Chart 1), a dinuclear compound of similar structure with a macrocycle made up of an N_3O_2 donor set.[4] The Mn(II)···Mn(II) distance in $[Mn_2(L1)Cl_4]$ is 11.18 Å, similar to the corresponding distance of 11.2 Å observed in the related $[Mn(N_3O_2)]_2$.[4] In the reduced form $[Mn_2(L2)Cl_4]$, the Mn(II)···Mn(II) distance is slightly larger (11.35 Å). The crystal packing of $[Mn_2(L1)Cl_4]$ and $[Mn_2(L2)Cl_4]$ can be seen in Figures S3 and S4, respectively.

Table 3. Selected Bond Angles (deg) and Torsion Angles (deg) for Molecular Structures of $[Mn_2(L1)Cl_4]\cdot 4MeOH$ and $[Mn_2(L2)Cl_4]\cdot 4MeOH$[a]

	$[Mn_2(L1)Cl_4]$	$[Mn_2(L2)Cl_4]$
Cl1−Mn1−Cl1B	177.3(9)	175.0(10)
N1−Mn1−N2	69.35(8)	71.65(18)
N1−Mn1−N2A/B	69.36(8)	71.65(18)
N2−Mn1−N3	73.08(12)	74.7(5)
N2A/B−Mn1−N3A/B	73.07(12)	71.5(7)
N3−Mn1−N3A	75.55(18)	75.5(5)
Cl2−Mn2−Cl2A/B	177.62(6)	173.7(9)
N4−Mn2−N5	69.42(7)	70.28(8)
N4−Mn2−N5A	69.42(7)	70.28(8)
N5−Mn2−N6	66.8(2)	73.66(12)
N5A−Mn2−N6A	66.8(2)	73.66(12)
N6−Mn2−N6A	89.8(5)	73.72(18)
C2−C1−C9−C10	28.4(2)	19.8(2)

[a]Symmetry transformations used to generate equivalent atoms: $-x + 1, y, -z + {}^1/_2$.

SQUID Measurements. Temperature dependent magnetic susceptibility measurements for $[Mn_2(L1)Cl_4]$ and $[Mn_2(L2)Cl_4]$ were performed at the applied field 1 T in the temperature range 2−300 K (Figure 2). The experimental data were fitted using a spin-Hamiltonian approach, eq 1:[40]

$$\hat{\mathbf{H}} = \mu_B \mathbf{g}_1 \hat{\mathbf{S}}_1 \mathbf{B} + \mu_B \mathbf{g}_2 \hat{\mathbf{S}}_2 \mathbf{B} - 2J \hat{\mathbf{S}}_1 \hat{\mathbf{S}}_2 \quad (1)$$

The first two terms represent an electron Zeeman effect for two paramagnetic centers, and the third term accounts for intramolecular interactions between them. The g-values for all high-spin d^5 ions were fixed to 2.00, whereas the effect of zero-field splitting operating on each $S_{Mn} = {}^5/_2$ was omitted to exclude overparameterization but to estimate the strength of intramolecular Mn(II)···Mn(II) interactions.

The effective magnetic moment, μ_{eff}, of 8.0 μ_B is almost constant in the temperature range 40−300 K for $[Mn_2(L2)Cl_4]$. At lower temperatures it gradually decreases due to weak antiferromagnetic intramolecular $S_{Mn} = {}^5/_2 \cdots S_{Mn} = {}^5/_2$ interactions and/or zero-field splitting effect. Complex $[Mn_2(L1)Cl_4]$ shows similar behavior, but with a lower plateau at μ_{eff} = 7.8 μ_B. This is lower than the value calculated for two noninteracting $S = {}^5/_2$ centers (8.37 μB, spin only approximation). Thus, diamagnetic impurity was included in simulations to account for the lower than predicted magnetic moments. The diamagnetic impurities are likely due to difficulty of removing solvent molecules left in the microcrystalline samples of $[Mn_2(L1)Cl_4]$ and $[Mn_2(L2)Cl_4]$ (see the elemental analyses and crystal structures).

Exchange coupling constants J were estimated to be smaller than -0.1 cm^{-1} for both complexes (Figure 2). Obviously, the coupling should be even weaker if one takes into account zero-field splitting effect for $S_{Mn} = {}^5/_2$ ions. Thus, according to the results of the magnetic susceptibility measurements, the two

dx.doi.org/10.1021/ic301714d | Inorg. Chem. 2013, 52, 222−236

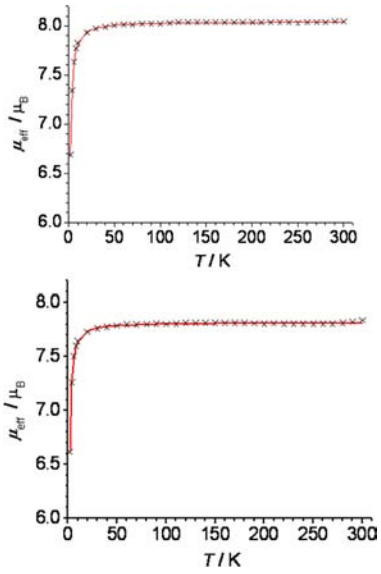

Figure 2. Temperature dependence of the effective magnetic moment μ_{eff} of a microcrystalline sample of $[Mn_2(\mathbf{L1})Cl_4]$ (bottom) and $[Mn_2(\mathbf{L2})Cl_4]$ (top) recorded at 1 T. The solid line in red represents the best fit obtained with $S_1 = S_2 = {}^5/_2$, $g_1 = g_2 = 2.00$ (fixed); diamagnetic impurities = 12.7%$_{weight}$ for $[Mn_2(\mathbf{L1})Cl_4]$ with $J = -0.04$ cm^{-1}; for $[Mn_2(\mathbf{L2})Cl_4]$, $J = -0.06$ cm^{-1}, diamagnetic impurities = 7.6%$_{weight}$.

high-spin Mn(II) centers in both $[Mn_2(\mathbf{L1})Cl_4]$ and $[Mn_2(\mathbf{L2})Cl_4]$ are essentially electronically uncoupled as it is also seen in the only comparable dinuclear high-spin Mn(II) complex known in the literature with a 4,4′-bipyridylic backbone, namely $[Mn(N_3O_2)]_2$.[4]

Potentiometric Titrations. In order to study the water exchange on the manganese(II) centers of $[Mn_2(\mathbf{L1})Cl_4]$ and $[Mn_2(\mathbf{L2})Cl_4]$ it was necessary to determine the speciation of both complexes in aqueous solutions. The axial chlorido ligands are very labile and replaced by water molecules as was shown by relaxivity[39] and conductivity[41] measurements (under conditions of $[Cl^-] = 250$ mM)[39] on complexes of a similar structure.[17,39] Recent studies have indicated coordination of one chloride atom to the Mn(II) center of a mitochondria-targeted SOD mimetic.[16] However, our ^{17}O NMR measurements in the presence of 300 mM chloride anions (see Supporting Information Table S11) showed no significant difference in the line broadening in comparison to the measurements in the absence of excess chloride concentrations confirming previous findings in similar systems (*vide supra*). Thus, no indication of Cl^- coordination to the manganese centers in $[Mn_2(\mathbf{L1})Cl_4]$ and $[Mn_2(\mathbf{L2})Cl_4]$ could be found under the applied experimental conditions (*vide infra*).

The calculated species distribution obtained from the best fits to the titration data are shown in Figure 3. On the basis of the number of species observed in the titration measurements, as well as the large distance between the two Mn(II) centers in the rigid ligand scaffolds, it can be concluded that the two macrocyclic subunits within both dinuclear complexes behave chemically identical to and independently from each other, as indicated by the SQUID analysis. For the fitting procedure the ligand was also treated as being an adduct of two identical mononuclear ligand motifs and not as a single dimeric unit, since the latter data treatment gave much larger errors and inaccurate pK values in the fitting process. The free **L2** ligand protonation constants (pK_1, pK_2, and pK_3) and the pK_a values of the coordinated water molecules (pK_{a1} and pK_{a2}) for $[Mn_2(\mathbf{L2})(H_2O)_4]^{4+}$, as well as the constants for water addition (pK(OH)$_1$ and pK(OH)$_2$) to the imine bonds of $[Mn_2(\mathbf{L1})(H_2O)_4]^{4+}$, together with the stability constants (log KM_2L and log KM_2H_2L) of both complexes are summarized in Table 4.

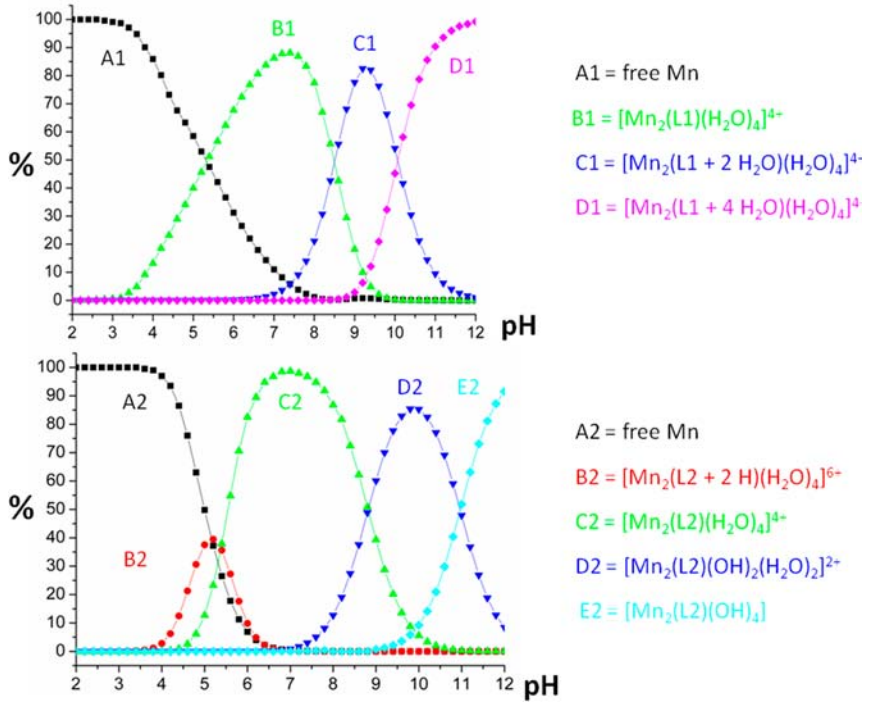

Figure 3. Species distribution for the complexes $[Mn_2(\mathbf{L1})(H_2O)_4]^{4+}$ (top) and $[Mn_2(\mathbf{L2})(H_2O)_4]^{4+}$ (bottom) as a function of pH at 25 °C and [complex] = 1 mM.

dx.doi.org/10.1021/ic301714d | *Inorg. Chem.* 2013, 52, 222−236

Table 4. pMn Values, Stability Constants and p*K* Values for the Studied Dinuclear and Analogous Mononuclear Complexes and Their Corresponding Ligands Determined by Potentiometric Titration at 25 °C

	dinuclear complexes		monuclear complexes[a]		
	$[Mn_2(\mathbf{L1})(H_2O)_4]^{4+}$	$[Mn_2(\mathbf{L2})(H_2O)_4]^{4+}$		$[Mn(Me_2\text{-Pyene})(H_2O)_2]^{2+}$	$[Mn(Me_2\text{-Pyane})(H_2O)_2]^{2+}$
pK_1[b]		5.01	pK_1[b]		5.24
pK_2[b]		8.03	pK_2[b]		9.35
pK_3[b]		10.81	pK_3[b]		9.96
$pK(OH)_1$	8.64		$pK(OH)_1$	7.62	
$pK(OH)_2$	10.10		$pK(OH)_2$	9.84	
pK_{a1}		8.92	pK_{a1}		
pK_{a2}		11.09	pK_{a2}		
log KM_2H_2L[c]		5.51	log $KMHL$[c]		5.66
logKM_2L[d]	8.42	8.83	log KML[e]	10.50	10.96
pMn[f]	3.8	6.1	pMn[f]	3.5	4.9

[a]Values for $[Mn(Me_2\text{-Pyene})(H_2O)_2]^{2+}$ from ref 25 and for $[Mn(Me_2\text{-Pyane})(H_2O)_2]^{2+}$ from this work, see Supporting Information Figure S5. [b]Ligand p*K* values. [c]In this case where the two macrocyclic subunits of the dinuclear complex behave chemically identically and independently from each other $KM_2H_2L = K_{MHL} = [MHL]/[ML][H]$. [d]$KM_2L = [M_2L]/[M]^2[L]$. [e]$K_{ML} = [ML]/[M][L]$. [f]$pMn = -\log[Mn(II)]_{free}$ (values calculated for $c_{complex}$ = 1 mM and pH = 7.4).

For comparison, the corresponding values for the mononuclear $[Mn(Me_2\text{-Pyene})(H_2O)_2]^{2+}$ and $[Mn(Me_2\text{-Pyane})(H_2O)_2]^{2+}$ complexes are also given in Table 4. The dinuclear imine complex shows solution behavior similar to its mononuclear analogue $[Mn(Me_2\text{-pyene})(H_2O)_2]^{2+}$,[25] and does not have a stable protonated form. Protonation of the ligand would lead to an imine hydrolysis,[25] and consequently decomposition of the pentadentate macrocyclic units, causing release of Mn(II) ions. At pH 7.5 the predominant species in solution was found to be the one with two aqua ligands attached to each manganese(II) center, $[Mn_2(\mathbf{L1})(H_2O)_4]^{4+}$. In the basic region, the base-catalyzed water addition to the imine double bonds to the carbinol derivatives occurs in two consecutive steps,[25] characterized by equilibrium constants $K(OH)_1$ and $K(OH)_2$ (Table 4). It should be mentioned that each of these two steps involves simultaneous addition of two water molecules, i.e., one to each macrocyclic unit.

The amine complex is more stable in acidic solutions than the imine complex and has a stable protonated form ($[Mn_2(\mathbf{L2} + 2H)(H_2O)_4]^{6+}$ with a maximal distribution at ca. pH = 5.0 (Figure 3 and Table 4), where protonation occurs at one of the secondary amine groups of both macrocyclic subunits. Similar species are observed in the same pH range with the analogous mononuclear complexes, but in significantly lower yields.[25] A direct comparison of the stability constants for the dinuclear and mononuclear complexes is not straightforward. Therefore, we calculated pMn ($-\log[Mn]_{free}$) values at pH = 7.4 and [complex] = 1 mM (Table 4). The higher pMn value for $[Mn_2(\mathbf{L2})(H_2O)_4]^{4+}$ (pMn = 6.1) than for $[Mn(Me_2\text{-Pyane})(H_2O)_2]^{2+}$ (pMn = 4.9)[17] indicates an order of magnitude smaller concentration of free Mn(II) ions in the solutions of dinuclear complex than in the solutions of its mononuclear analogue at pH 7.4, demonstrating that the dinuclear structure provides a higher complex stability. This is different from what has been observed in the case of dinuclear $[Mn_2(ENOTA)(H_2O)_2]$, which is less stable than the corresponding mononuclear complexes, due to the reduced number of carboxylate groups that thermodynamically stabilize the Mn(II) center.[17] However, $[Mn_2(\mathbf{L2})(H_2O)_4]^{4+}$ is less stable than the six-coordinate $[Mn_2(ENOTA)(H_2O)]$ complex (pMn = 7.7).[17]

The acidity of the coordinated water molecules in $[Mn_2(\mathbf{L2})(H_2O)_4]^{4+}$, with pK_{a1} = 8.92 for deprotonation of the first set of aqua ligands and pK_{a2} = 11.09 for deprotonation of the second set of aqua ligands from both macrocyclic subunits, is significantly higher than in $[Mn(Me_2\text{-Pyane})(H_2O)_2]^{2+}$ (Figure S5) . In the case of mononuclear hydroxo species, their formation is followed by complex decomposition and MnO_2 precipitation. On the other hand, ca. 85% of $[Mn_2(\mathbf{L2})(OH)_2(H_2O)_2]^{2+}$ and 10% of $[Mn_2(\mathbf{L2})(OH)_4]$ exist at pH 10.0. To best of our knowledge, $[Mn_2(\mathbf{L2})(OH)_2(H_2O)_2]^{2+}$ is the first example of a stable *trans*-aqua-hydroxo manganese(II) species in solution, a discovery that highlights the potential for synthetically tuning the lability of coordinated water molecules in manganese(II) complexes. In comparison, neutral $[Mn_2(ENOTA)(H_2O)_2]$, which is the only reported dinuclear manganese(II) complex with inner sphere water molecules, also forms hydroxo species (15% of $[Mn_2(ENOTA)(H_2O)_2]$, 25% of $[Mn_2(ENOTA)(OH)(H_2O)]^-$, and 60% of $[Mn_2(ENOTA)(OH)_2]^{2-}$ at pH = 10.0).[17] Different from $[Mn_2(\mathbf{L2})(OH)_2(H_2O)_2]^{2+}$, the aqua and hydroxo ligands do not belong to the coordination sphere of the same manganese(II) center in $[Mn_2(ENOTA)(OH)(H_2O)]^-$, where only one aqua ligand can be coordinated to a manganese(II) center due to the octahedral geometry of this complex.[17]

ESI Mass Measurements. To further characterize species in aqueous solutions of different pH values we performed ultrahigh-resolution ESI mass spectrometry combined with cold spray ionization. A complete overview for the main species of $[Mn_2(\mathbf{L2})Cl_4]$ observed at different pH values is given in Table 5. Analysis of the spectra showed that the dinuclear amine complex remained intact under the applied ESI conditions (main species at m/z 769.2163 for $[Mn_2(\mathbf{L2})Cl_3]^+$, Figure 4, Table 5), whereas for the dinuclear imine complex $[Mn_2(\mathbf{L1})Cl_4]$ a minor decomposition product could be identified even at pH = 7.5 (see Supporting Information Figures S6 and S7). This is in agreement with the lower stability of manganese(II) imine complexes compared to their reduced amine analogues. Due to the high affinity of the manganese(II) centers toward chloride anions under conditions within the mass spectrometer, the main MS peaks at neutral pH values correspond to the chloride adducts (Table 5, Figure 4). However, at pH 10.0 and 4 °C we were able to identify the hydroxo species as well (m/z 348.1592, Table 5, Figure 5). Under the applied ESI conditions, deprotonation of the secondary amine groups was also observed at pH = 10.0 (m/z 330.1418 and 348.1362, Figure

dx.doi.org/10.1021/ic301714d | *Inorg. Chem.* 2013, 52, 222−236

Table 5. UHR-ESI-MS Data at Various pH Values and Temperatures Corresponding to the Intact Complexes of $[Mn_2(L2)X_aY_b]^{z+a}$

recorded m/z	calcd m/z^b	peak assignement	pH	temp
769.2163	769.2170	$[Mn_2(L2)Cl_3]^+$	7.0	180 °C
330.1418	330.1481	$[Mn_2(L2-2H^+)]^{2+}$	10.0	4 °C
339.1534	339.1537	$[Mn_2(L2-H^+)(OH)]^{2+}$	10.0	4 °C
348.1362	348.1368	$[Mn_2(L2-H^+)Cl]^{2+}$	10.0	4 °C
348.1592	348.1591	$[Mn_2(L2)(OH)_2]^{2+}$	10.0	4 °C
357.1416	357.1421	$[Mn_2(L2)(OH)Cl]^{2+}$	10.0	4 °C
366.1246	366.1252	$[Mn_2(L2)Cl_2]^{2+}$	10.0	4 °C

[a]Only signals with a relative intensity ≥10% are given. (X = Cl, OH; Y = Cl, OH; a = 0, 1, 2; b = 0, 1, 2; z = 1, 2). [b]Simulation was performed with the Bruker data analysis 4.0 software.

5, Table 5). Deprotonation of coordinated secondary amines is known in the literature.[42]

^{17}O NMR Measurements. The obtained ^{17}O NMR data have been fitted according to the equation developed by Swift and Connick.[43] (For full experimental data, details of data treatment, and calculation of the water exchange parameters summarized in Tables 6 and 7, see Supporting Information). The water exchange measurements of the imine complex were performed at pH 7.5 and 9.3, where the predominant species in noncoordinating aqueous buffers are tetraaqua-species of the complex in the imine $[Mn_2(\mathbf{L1})(H_2O)_4]^{4+}$ form and in the carbinol $[Mn_2(\mathbf{L1}+2H_2O)(H_2O)_4]^{4+}$ form resulting from water addition to an imine double bound on each of the dinuclear units, respectively (Figure 3). The measurements on the amine complex were performed at pH 7.0, 10.0, and 11.0, where the complex predominantly exists as the tetraaqua ($[Mn_2(\mathbf{L2})(H_2O)_4]^{4+}$) and diaqua-dihydroxo ($[Mn_2(\mathbf{L2})(OH)_2(H_2O)_2]^{2+}$) species, respectively (Figure 3). For the data analysis the two manganese centers were considered to behave independently, as supported by our SQUID and potentiometric titration studies (*vide supra*). All rate constants and water-exchange parameters for the temperature and pressure dependent measurements are summarized in Table 6. The temperature range for the measurements of the imine complex was 274.2−338.2 K, since we observed some decomposition of the complex at elevated temperatures, especially at pH 9.3. In the case of the amine complex a broader temperature window could be used (274.2−358.2 K) since no decomposition was observed. The water exchange rate constants are not significantly different for $[Mn_2(\mathbf{L1})(H_2O)_4]^{4+}$ and $[Mn_2(\mathbf{L1}+2H_2O)(H_2O)_4]^{4+}$ at pH 7.5 and 9.3, respectively. They are also very close to the values obtained for the mononuclear analogue at corresponding pH (Table 7), where pH has no influence on the water exchange process, as well. In the carbinol form of the **L1** ligand (**L1** + $2H_2O$), the electronegativity of the hydroxo group counters the decrease in π-acceptor ability of the macrocycle, and as a result the carbinol pentadentate system has similar electronic properties to the imine macrocycle.[25] A decreased π-acceptor ability of the amine **L2** ligand in comparison to imine **L1** results in certain labilization of the axially coordinated water molecules in $[Mn_2(\mathbf{L2})(H_2O)_4]^{4+}$. At pH 10.0, where the aqua-hydroxo complex $[Mn_2(\mathbf{L2})(OH)_2(H_2O)_2]^{2+}$ is the predominant species according to the potentiometric measurements (*vide supra*), the observed exchange rate is higher than for the tetraaqua species at pH 7.0. This confirms the *trans*-aqua-hydroxo coordination on both Mn(II), because otherwise, in a hypothetical asymmetrical coordination with two water molecules on one Mn(II) and two hydroxo groups on another manganese(II) center, there would be no change in k_{ex}. The species distribution and hydration number of the manganese center is consistent with the typically observed ^{17}O NMR line broadening seen for similar complexes[39] and is also affirmed by the fact that the water exchange at pH 10.0 for $[Mn_2(\mathbf{L2})(H_2O)_4]^{4+}$ would be much slower if calculated for four labile aqua ligands instead of two and would not fit the experimentally obtained data. Additionally, the hyperfine

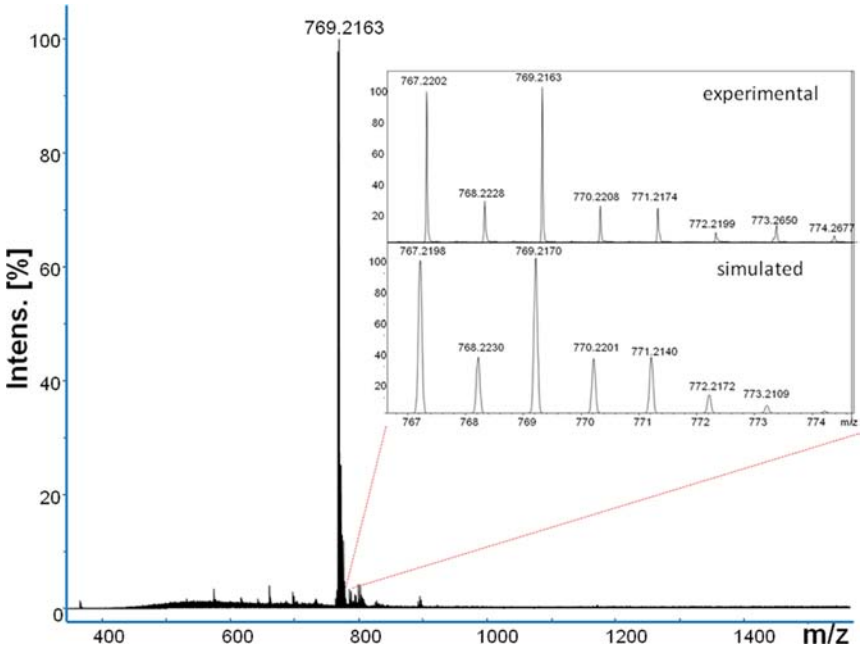

Figure 4. High accuracy mass spectrum of $[Mn_2(\mathbf{L2})Cl_4]$ at 180 °C in aqueous solution pH 7.0. Main species at m/z 769.2163 is assigned to $[Mn_2(\mathbf{L2})Cl_3]^+$. Insert shows measured spectra (top) of main species and simulated isotopic pattern thereof (bottom).

dx.doi.org/10.1021/ic301714d | *Inorg. Chem.* 2013, 52, 222−236

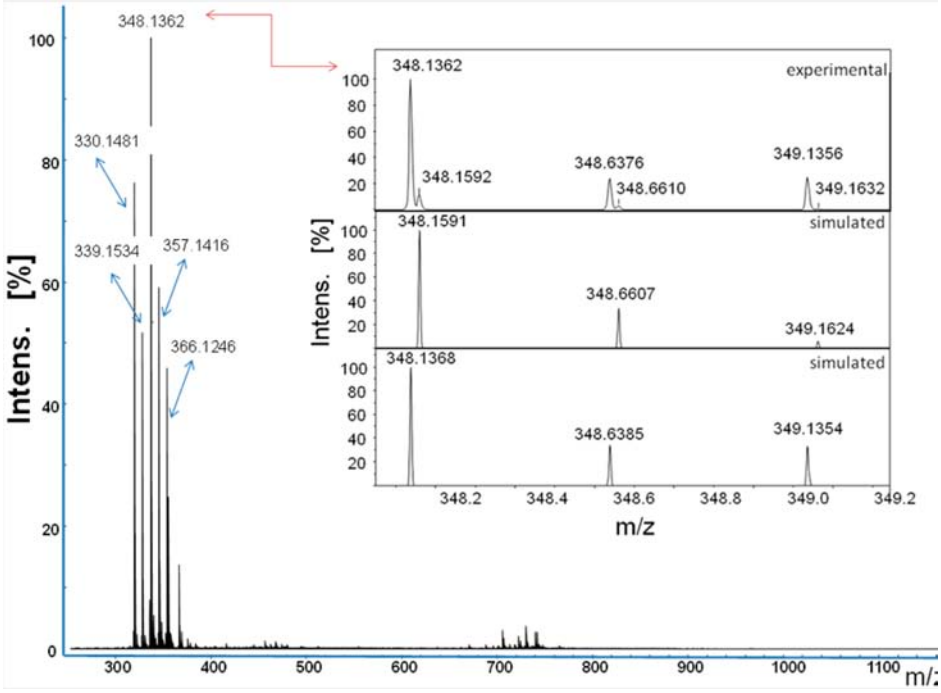

Figure 5. High accuracy mass spectrum at 4 °C in aqueous solution at pH 10.0. Insert: Two species at m/z 348.1362 and m/z 348.1592. Top is measured spectra, middle is simulated isotopic pattern for $[Mn_2(\mathbf{L2})(OH)_2]^{2+}$ species, and bottom is simulated pattern for $[Mn_2(\mathbf{L2}-H^+)Cl]^{2+}$.

Table 6. Best Fit Parameters for Water Exchange from Temperature Dependent ^{17}O NMR Measurements

parameter	$[Mn_2(\mathbf{L1})(H_2O)_4]^{4+}$	$[Mn_2(\mathbf{L1}+2H_2O)(H_2O)_4]^{4+}$	$[Mn_2(\mathbf{L2})(H_2O)_4]^{4+}$	$[Mn_2(\mathbf{L2})(OH)_2(H_2O)_2]^{2+}$	$[Mn_2(\mathbf{L2})(OH)_2(H_2O)_2]^{2+}$
pH	7.5[a]	9.3[b]	7.0[a]	10.0[b]	11.0[b]
k_{ex}^{298} [$\times 10^7$ s^{-1}]	1.7 ± 0.3	1.5 ± 0.3	5.0 ± 0.4	7.1 ± 0.6[c]	3.0 ± 0.5[c]
$\Delta H^{\ddagger}$ [kJ mol^{-1}]	34.5 ± 1.3	36.6 ± 1.1	32.9 ± 1.9	36.5 ± 1.9	44.9 ± 3.2
$\Delta S^{\ddagger}$ [J mol^{-1} K^{-1}]	+9.2 ± 3.0	+15.4 ± 2.1	+12.8 ± 6.1	+27.8 ± 7.1	+48.8 ± 12.5
Δ [$\times 10^{10}$ rad s^{-1}]	1.0 ± 0.3	1.3 ± 0.5	1.7 ± 0.6	1.2 ± 0.5	1.3 ± 0.7
τ_v^{298} [$\times 10^{-12}$ s^{-1}]	1.8 ± 0.3	1.9 ± 0.4	2.8 ± 0.3	1.4 ± 0.6	1.6 ± 0.8
A/h [$\times 10^6$ s^{-1}]	6.0[d]	6.0[d]	6.1 ± 0.2	6.0 ± 0.3	5.6 ± 1.0

[a]In 0.2 M PIPES buffer. [b]In 0.2 M CAPS buffer. [c]k_{ex} = 8.0 × 10^7 s^{-1} is estimated for pure $[Mn_2(\mathbf{L2})(OH)_2(H_2O)_2]^{2+}$. [d]For $Mn_2\mathbf{L1}$ the hyperfine coupling constant was fixed to a reasonable value, i.e., the one obtained for $Mn_2\mathbf{L2}$, since it could not be determined correctly with fitting, as the system is in the slow exchange region.

Table 7. Water Exchange Parameters and Exchange Rates Obtained by Temperature and Pressure Dependent ^{17}O NMR Measurements for $[Mn_2(\mathbf{L1})(H_2O)_4]^{4+}$, $[Mn_2(\mathbf{L2})(H_2O)_4]^{4+}$, and Mononuclear Mn(II) Complexes

compound	pH	k_{ex}^{298} [$\times 10^7$ s^{-1}]	$\Delta H^{\ddagger}$ [kJ mol^{-1}]	$\Delta S^{\ddagger}$ [J mol^{-1} K^{-1}]	$\Delta V^{\ddagger}$ [cm^3 mol^{-1}]	ref
$[Mn_2(\mathbf{L1})(H_2O)_4]^{4+}$	7.5	1.7 ± 0.2	34.5 ± 1.3	+9.2 ± 3.0	+4.1 ± 0.2[a]	this work
$[Mn_2(\mathbf{L1}+2H_2O)(H_2O)_4]^{4+}$	9.3	1.5 ± 0.3	36.6 ± 1.1	+15.4 ± 2.1	+3.8 ± 0.2[b]	this work
$[Mn_2(\mathbf{L2})(H_2O)_4]^{4+}$	7.0	5.0 ± 0.4	32.9 ± 1.9	+12.8 ± 6.1	+3.4 ± 0.2[c]	this work
$[Mn_2(\mathbf{L2})(OH)_2(H_2O)_2]^{2+}$	10.0	7.1 ± 0.3	36.5 ± 1.9	+27.8 ± 7.1	+5.4 ± 0.3[d]	this work
$[Mn_2(\mathbf{L2})(OH)_2(H_2O)_2]^{2+}$	11.0	3.0 ± 0.5[e]	44.9 ± 3.2	+48.8 ± 12.5	n.d.	this work
$[Mn(Me_2\text{-}Pyene)(H_2O)_2]^{2+}$	7.6	1.7 ± 0.1	35.9 ± 1.7	+23.6 ± 5.8	n.d.	25
$[Mn(Me_2\text{-}Pyene)(H_2O)_2]^{2+}$	9.5	1.6 ± 0.1	39.5 ± 1.1	+25.7 ± 3.8	+5.3 ± 0.2	25
$[Mn(Me_2\text{-}Pyane)(H_2O)_2]^{2+}$	7.7	5.3 ± 0.3	37.2 ± 0.4	+27.6 ± 1.5	+5.2 ± 0.7	25
$[Mn(Me_2\text{-}Pyane)(H_2O)_2]^{2+}$	10.9	5.8 ± 0.3	33.3 ± 0.6	+15.2 ± 1.9	+3.4 ± 0.7	25
$[Mn_2(ENOTA)(H_2O)_2]$	8.0	5.5 ± 0.9	20.5 ± 1.6	−28.0 ± 6.0	−10.7 ± 1.1	17
$[Mn(H_2O)_6]^{2+}$	~1	2.1 ± 0.1	32.9 ± 1.3	+5.7 ± 5.0	−5.4 ± 0.1	52

[a]At 290.2 K. [b]At 290.2 K. [c]At 335.2 K. [d]At 335.2 K. [e]k_{ex} = 8.0 × 10^7 s^{-1} is estimated for pure $[Mn_2(\mathbf{L2})(OH)_2(H_2O)_2]^{2+}$.

coupling constant (A/h) obtained via the fitting of the reduced transverse relaxation rates (see SI) is sensitive to the number and the nature of the donor atoms in close proximity of the paramagnetic Mn(II).[14,39] The obtained value is consistent with typical Mn(II)−O interaction values (4.2 −2.0 × 10^6 s^{-1})[39,44] only under consideration that the number of exchanged water molecules for $[Mn_2(\mathbf{L2})]^{z+}$ is n = 4 and n = 2 at pH = 7.0 and pH = 10.0, respectively. All other possible combinations with different hydration numbers at the respective pH values resulted not only in unreasonable $1/T_{2r}$ values (based on

dx.doi.org/10.1021/ic301714d | Inorg. Chem. 2013, 52, 222−236

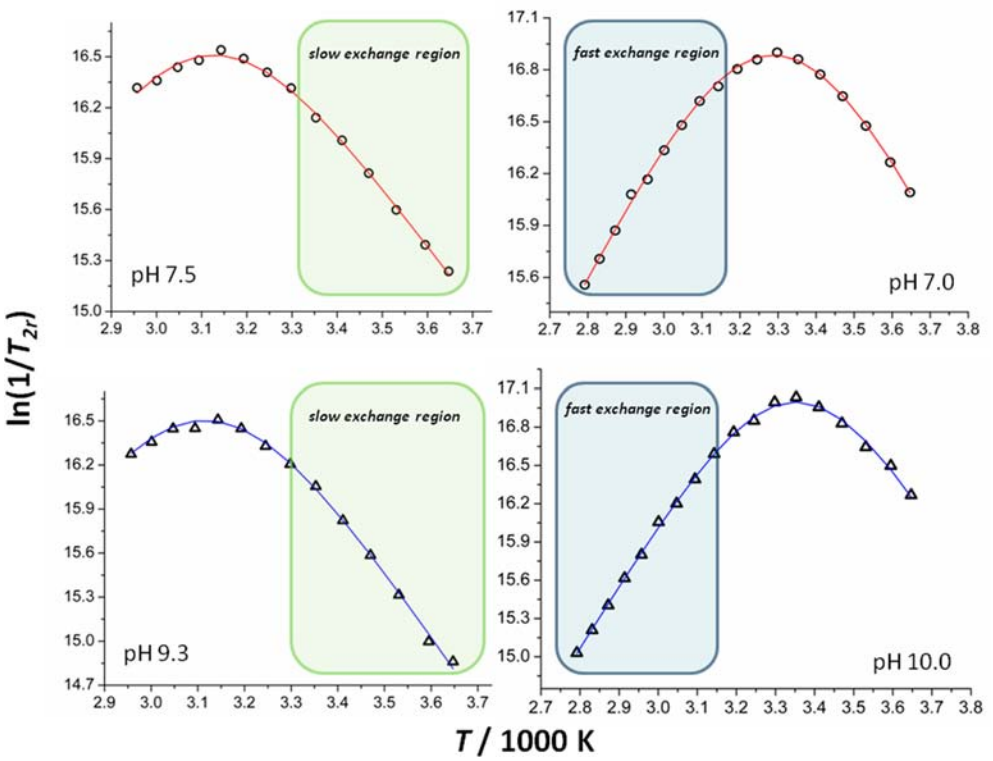

Figure 6. Plots of $\ln(1/T_{2r})$ data for $[Mn_2(\mathbf{L1})(H_2O)_4]^{4+}$ (pH 7.5, top left) or $[Mn_2(\mathbf{L1}{+}2H_2O)(H_2O)_4]^{4+}$ (pH 9.3, bottom left) and $[Mn_2(\mathbf{L2})(H_2O)_4]^{4+}$ (pH 7.0, top right) or $[Mn_2(\mathbf{L2})(OH)_2\ (H_2O)_2]^{2+}$ (pH 10.0, bottom right) versus reciprocal temperature obtained from ^{17}O NMR measurements. For full experimental data and data treatment see SI.

literature values reported for Mn(II) systems) but also in implausible scalar hyperfine coupling constants, vastly different from that already reported in literature for a Mn(II)−O interaction.[39,47,50,52] Furthermore, to confirm the character of species formed at pH higher than 10.0, we measured the rate of water exchange at pH 11.0 (Figure S8 and Table S10). The observed decrease of k_{ex} (Table 6) clearly indicates that under these conditions deprotonation of the other two aqua ligands occurs, resulting in a tetrahydroxo species that is substitution inert within the time scale of the performed measurements. In contrast, deprotonation of the amine **L2** ligand instead of aqua ligands would increase electronic density on Mn(II) and consequently increase the exchange rate of the remaining aqua ligands due to enhanced lability of the axial metal−water bonds, which is a well-known effect of spectator ligands with relatively higher negative charge.[45] Thus, the deprotonation of **L2** detected by ESI MS is due to the experimental conditions specific to those experiments. (Table 5, Figure 5).

Considering that at pH 10.0 there is 85% of $[Mn_2(\mathbf{L2})(OH)_2(H_2O)_2]^{2+}$, 5% of tetraaqua, and 10% of substitution inert tetrahydroxo species (Figure 3), the water exchange rate constant of the pure aqua-hydroxo complex is calculated to be ca. $8 \times 10^7\ s^{-1}$. Thus, for the first time we could determine the *trans*-effect of the hydroxo group on the water exchange process on a manganese(II) center. The *trans*-hydroxo ligand caused just a 1.6-fold increase in the water exchange rate on Mn(II). In general a significant increase in exchange rate of the *trans*-aqua ligand is observed for a variety of octahedral *trans*-aqua-hydroxo trivalent metal species, for which water exchange is 10^2 to 10^4 times faster than on corresponding *trans*-diaqua species.[46,47] (The Mn(III) aqua-hydroxo octahedral porphyrin complexes, where also only ca. a 1.6-fold increase in the water exchange rate was observed, are just an exception.)[48] A possible reason why there is a much smaller difference in aqua ligand exchange between the $[Mn_2(\mathbf{L2})(OH)_2(H_2O)_2]^{2+}$ and $[Mn_2(\mathbf{L2})(H_2O)_4]^{4+}$ complexes is that the Mn(II)−OH_2 bonds in the $[Mn_2(\mathbf{L2})(H_2O)_4]^{4+}$ complex are longer than those found in the trivalent metal complexes and are thus less sensitive to the *trans*-hydroxide effect. However, whether the weak *trans*-labilization effect of the hydroxo ligand in $[Mn_2(\mathbf{L2})(OH)_2(H_2O)_2]^{2+}$ is characteristic of hepta-coordinate Mn(II) or it is a more general feature of Mn(II) and/or divalent metal centers remains to be seen.

The values obtained for activation enthalpies, $\Delta H^{\ddagger}$, are all in the same range as those reported in the literature for the corresponding mononuclear complexes (Table 7).[25] The values for the activation entropies are all positive and similar to those obtained for mononuclear analogues, which suggests a dissociative interchange mechanism (I_d) for the water exchange on seven-coordinate Mn(II) in general. In order to get a better insight into the water-exchange mechanism of the two dinuclear complexes we additionally performed pressure dependent ^{17}O NMR studies, as the derived activation volume, $\Delta V^{\ddagger}$, is a much more sensitive and reliable parameter for the elucidation of the nature of water exchange mechanism, since usually the activation entropy $\Delta S^{\ddagger}$ is subjected to a larger experimental error.[47,49] The pressure dependence of k_{ex} is given by eq 2, where k_{ex}^{0} is the rate constant for the solvent exchange at zero pressure and the activation volumes (Table 7) were obtained by fitting the data by eq 2 and to the equations describing $1/T_{2r}$ relaxation (see SI). The parameters A/h and τ_v were considered pressure independent for the fast exchanging system, since the calculated contribution of electronic relaxation $1/T_{1e}$ to $1/T_{2r}$ at elevated temperatures is small (about 7% at 335.2 K for

dx.doi.org/10.1021/ic301714d | *Inorg. Chem.* 2013, 52, 222−236

$[Mn_2(\mathbf{L2})Cl_4]$) and a pressure dependence of $1/T_{1e}$ would therefore have small to negligible effects on the calculated activation volume (see literature).[50,51]

$$\frac{1}{\tau_m} = k_{ex} = k_{ex}^0 \exp\left(-\frac{\Delta V^{\ddagger}}{RT}p\right) \quad (2)$$

The pressure dependent studies on $[Mn_2(\mathbf{L1})Cl_4]$ at pH 7.5 and 9.5 were performed in the slow exchange region (Figure 6) at 288.2 K, where k_{ex} can be approximated by eq 3a. Consequently, the observed decrease in the transverse relaxation rate with increasing pressure (Figure 7, top) indicates

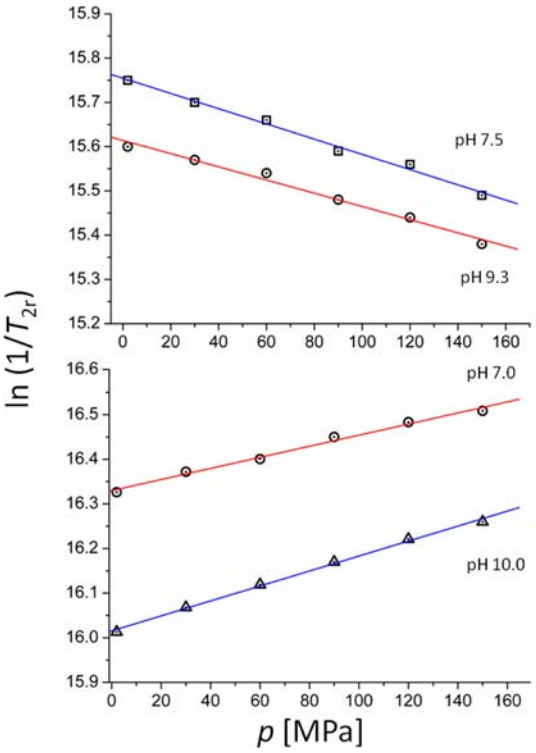

Figure 7. Pressure dependence of the reduced ^{17}O transverse relaxation. Top: $[Mn_2(\mathbf{L1})(H_2O)_4]^{4+}$ (pH 7.5) and $[Mn_2(\mathbf{L1}+2H_2O)(H_2O)_4]^{4+}$ (pH 9.3). Bottom: $[Mn_2(\mathbf{L2})(H_2O)_4]^{4+}$ (pH 7.0) and $[Mn_2(\mathbf{L2})(OH)_2(H_2O)_2]^{2+}$ (pH 10.0). Solid lines represent least-squares fit to the experimental data. For full experimental details see SI.

a dissociative water exchange process at both pH values, since the water exchange rate slows down with increasing pressure. The pressure dependent measurements for $[Mn_2(\mathbf{L2})Cl_4]$ at pH 7.0 and 10.0 were performed in the fast exchange region (Figure 6), where the relationship of k_{ex} to $1/T_{2r}$ is approximated by eq 3b. Therefore, the increase of $1/T_{2r}$ (Figure 7, bottom) indicates a slowdown of the water exchange rate with increasing pressure, pointing toward a dissociative exchange mechanism.

$$\frac{1}{T_{2r}} \cong \frac{1}{\tau_m} = k_{ex} \quad (3a)$$

$$\frac{1}{T_{2r}} \cong \tau_m \Delta\omega^2 = \frac{1}{k_{ex}}\Delta\omega^2 \quad (3b)$$

In all experiments the obtained activation volumes had small positive values (Table 6 and 7) indicative for an interchange dissociative water exchange mechanism, I_d. The fact that $\Delta V^{\ddagger}$ for $[Mn_2(\mathbf{L2})(OH)_2(H_2O)_2]^{2+}$ is only slightly bigger than that for $[Mn_2(\mathbf{L2})(H_2O)_4]^{4+}$ is in accordance with the weak *trans*-hydroxo effect that is not prominent enough to induce a mechanistic changeover from an interchange dissociative (I_d) toward a pure dissociative (D) mechanism. To date, the operation of a pure D-mechanism has not been reported for exchange processes in Mn(II) species. Even on the negatively charged pentagonal-bipyramidal $[Mn(EDTA)(H_2O)]^{2-}$ complex, where the aqua ligand is positioned in the sterically crowded equatorial plane containing five donor atoms, the water exchange proceeds by an I_d mechanism ($\Delta V^{\ddagger}$ =+3.4 ± 0.2 cm^3/mol).[51] On the other hand, water exchange in the six-coordinate Mn(II) species $[Mn(H_2O)_6]^{2+}$ and $[Mn_2(ENOTA)(H_2O)_2]$ favors an associative mechanism, as characterized by a negative volume of activation (Table 7) due to a relatively less steric crowding on the metal center.

Electrochemistry. To further investigate a possible electronic communication between the two manganese(II) centers within $[Mn_2(\mathbf{L1})Cl_4]$ and $[Mn_2(\mathbf{L2})Cl_4]$, their redox behavior in aqueous (60 mM PIPES buffer pH 7.0) and anhydrous (DMSO) solutions was investigated. The cyclic voltammogram of $[Mn_2(\mathbf{L1})Cl_4]$ in aqueous solution shows an oxidation peak at E_{ox} = 1.12 V versus NHE and a reduction peak at E_{red} = 0.62 V versus NHE. The broadness of the peaks along with the magnitude of the peak separation indicates an irreversible redox behavior. In contrast, the mononuclear $[Mn(Me_2\text{-}Pyene)Cl_2]$ complex shows a reversible process (E_{ox} = 0.88 V and E_{red} = 0.76 V vs NHE) which is assigned to the Mn(II)/Mn(III) redox couple (Figure 8). For the amine complexes, $[Mn_2(\mathbf{L2})Cl_4]$ (E_{ox} = 1.15 V and E_{red} = 0.59 V vs NHE) and its corresponding mononuclear analogue $[Mn(Me_2\text{-}Pyane)Cl_2]$ (E_{ox} = 1.14 V and E_{red} = 0.88 V vs NHE), similar electrochemical behavior was observed (Figure 8). The existence of a single oxidation and single reduction process in the case of dinuclear complexes and comparison of the cathodic and anodic peak intensities between mono- and dinuclear complexes confirm that the two manganese centers do not significantly communicate. Thus, the observed two-electron anodic and cathodic processes are related to the oxidation and reduction of two Mn centers within the dinuclear structures, respectively. The large peak separation could be due to a relatively low fexibility of the dinuclear complex which would require a higher reorganization energy to adapt to the electronic change and/or, in terms of an EC mechanism (electrochemical-chemical mechanism),[53] the deprotonation of the aqua ligands upon oxidation.[54] Due to the relatively broad peaks, the effect of pH on electrochemical behavior of dinuclear complexes could not be unambiguously assessed by cyclic voltammetry in aqueous solutions of higher pH. However, an increase of the peak separation with increased pH could be observed for $[Mn_2(\mathbf{L2})Cl_4]$ at pH 10.0 (E_{ox} = 1.15 V and E_{red} = 0.56 V vs NHE, Figure S11). Furthermore, the measurements in aprotic DMSO demonstrated an even larger peak separation and a prominent decrease of the corresponding cathodic peaks for both $[Mn_2(\mathbf{L1})Cl_4]$ and $[Mn_2(\mathbf{L2})Cl_4]$ (see Supporting Information Figures S9 and S10). These results suggest that protolytic reactions are involved in the underlying redox processes of the **L1** and **L2** complexes.

SOD Activity. The dinuclear $[Mn_2(\mathbf{L1})Cl_4]$ complex does not show any catalytic activity for superoxide dismutation, in accord with the known inactivity of mononuclear $[Mn(Me_2\text{-}Pyene)Cl_2]$.[25,55] In contrast to $[Mn_2(\mathbf{L1})Cl_4]$, the reduced

dx.doi.org/10.1021/ic301714d | *Inorg. Chem.* 2013, 52, 222−236

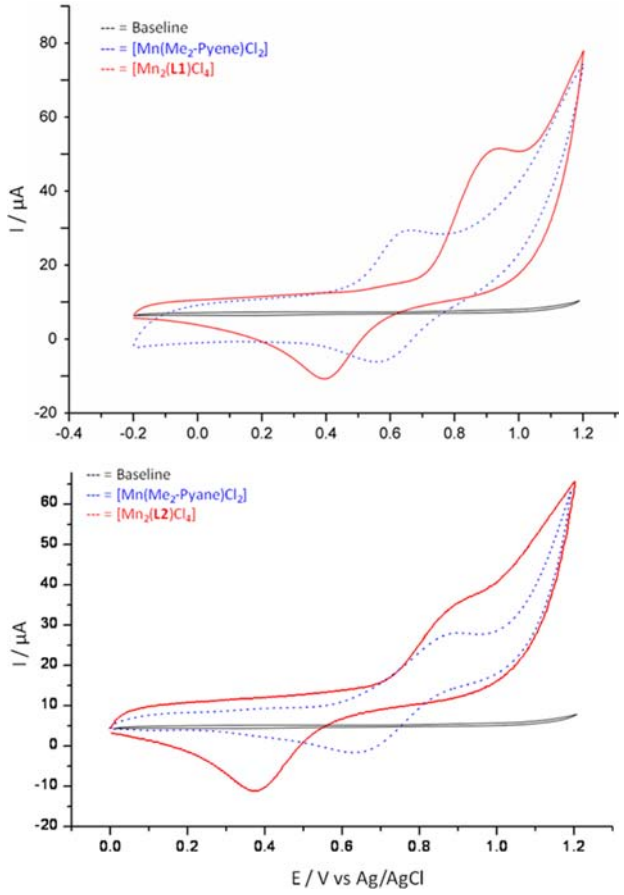

Figure 8. Cyclic voltammograms of $[Mn_2(\mathbf{L1})Cl_4]$ (top, solid red line) and $[Mn_2(\mathbf{L2})Cl_4]$ (bottom, solid red line) in 60 mM PIPES buffer at pH 7.0. Cyclic voltamogramms of the mononuclear complexes $[Mn(Me_2\text{-Pyene})Cl_2]$ (top) and $[Mn(Me_2\text{-Pyane})Cl_2]$ (bottom) are represented as dotted blue lines. All complexes were measured as 1 mM solutions under a N_2 atmosphere. Scan rate = 100 mV/s, temperature = 20 °C.

complex $[Mn_2(\mathbf{L2})Cl_4]$ shows SOD activity, which was determined at pH 7.4, 8.1, and 10.0 by direct stopped-flow measurements (Figure 9 and Tables 8 and S11–S14).[19] The obtained catalytic rate constants were compared with those for mononuclear $[Mn(Me_2\text{-Pyane})Cl_2]$ and with uncatalyzed superoxide dismutation rate constants at corresponding pH, as summarized in Table 8.

The observed SOD activity is approximately 2 times (within experimental error limits) higher for the dinuclear complex than for the mononuclear one at pH 7.4 and 8.1 (Table 8). This is due to the fact that the two Mn(II) centers behave independently from each other, as demonstrated by SQUID, potentiometric, electrochemical, and water exchange measurements. Under these conditions both complexes are predominantly present in the solutions as aqua species. At pH 10.0, where the dinuclear complex mostly exists in the $[Mn_2(\mathbf{L2})(OH)_2(H_2O)_2]^{2+}$ form, its k_{cat} is more than double that of the catalytic rate of the mononuclear analogue (Table 8). However, faster water exchange in $[Mn_2(\mathbf{L2})(H_2O)_4]^{4+}$ compared to mononuclear $[Mn(Me_2\text{-Pyane})]$ at pH 10.0 is not the reason for this. Namely, dissociation of an aqua ligand is not the rate determining step in the catalytic process, because the corresponding second-order rate constant for water exchange ($k_{ex}/[H_2O] = 1.3 \times 10^6\ M^{-1}\ s^{-1}$) is 1 order of magnitude lower

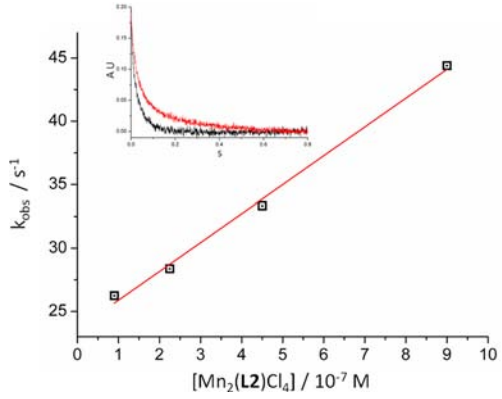

Figure 9. Plot of k_{obs} versus complex concentration for the reaction of a 2.0×10^{-4} M superoxide solution in DMSO with $[Mn_2(\mathbf{L2})(H_2O)_4]^{4+}$ in 60 mM HEPES buffer pH 8.1 at 21 °C and a DMSO-buffer mixing ratio 1:10, respectively. Inset: Trace at 250 nm for the reaction of 9.0×10^{-7} M $[Mn_2(\mathbf{L2})(H_2O)_4]^{4+}$ with 2.0×10^{-4} M KO_2 (black line) and self-decomposition of 2.0×10^{-4} M KO_2 under the same conditions (red line).

than k_{cat} at pH 10.0. A rate determining process (Scheme 3) has been proposed in the literature,[57] where a transient Mn(III)-peroxo intermediate oxidizes additional superoxide followed by fast protonation of the resultant Mn(II)-peroxide adduct. At higher pH the protonation is generally less favorable and might become involved in a rate determining step. Although there is some evidence in the literature for a concerted proton–electron transfer mechanism of the natural iron and manganese SOD enzymes[58] and a seven-coordinate iron SOD mimetic,[59] in the case of the herein studied class of pentaazamacrocyclic Mn(II) complexes a role of the proton transfer in a rate determining process within the catalytic SOD cycle is still unknown. However, we can speculate, in the light of our findings, that the existence of the hydroxo group in the coordination sphere of our dinuclear Mn(II) complex at pH 10.0 would increase pK_a of putative manganese(II)–peroxo intermediate. Consequently, the protonation and H_2O_2 release would be more feasible for $Mn(II)(OH)(O_2^{2-})$ than for the $Mn(II)(O_2^{2-})$ species. This may affect the catalytic SOD activity, especially in solutions of higher pH values, as our experiments have indicated.

These mechanistic considerations can explain the relatively higher SOD activity per manganese center of $[Mn_2(\mathbf{L2})(OH)_2(H_2O)_2]^{2+}$ than of $[Mn(Me_2\text{-Pyane})(H_2O)_2]^{2+}$ at pH 10.0.

CONCLUSION

Two dinuclear seven-coordinate manganese(II) complexes containing two pentaazamacrocyclic imine or amine-based subunits have been synthesized and characterized in the solid state and in aqueous solutions. Their solution behavior was investigated in detail by studying their speciation, redox behavior, water exchange at Mn(II) centers, and SOD activity.

On the basis of SQUID, potentiometric, electrochemical, and water exchange measurements, the two manganese(II) centers within the dinuclear structures of $[Mn_2(\mathbf{L1})Cl_4]$ and $[Mn_2(\mathbf{L2})Cl_4]$ behave independently from each other and similarly to the manganese centers in the corresponding mononuclear complexes. However, the dinuclear amine complex possesses increased complex stability and acidity of the coordinated water molecules ($pK_{a1} = 8.92$) in comparison to the corresponding mononuclear mononuclear analogue. This

dx.doi.org/10.1021/ic301714d | Inorg. Chem. 2013, 52, 222–236

Table 8. Second-Order Rate Constants k_{cat} at 21 °C for Catalytic Dismutation of Superoxide with $[Mn_2(L2)Cl_4]$ and $[Mn(Me_2\text{-Pyane})]$ and for Uncatalyzed Superoxide Dismutation at Different pH Values

	HEPES pH 7.4 [$\times 10^6$ M^{-1} s^{-1}]	ref	HEPES pH 8.1 [$\times 10^6$ M^{-1} s^{-1}]	ref	CAPS pH 10.0 [$\times 10^6$ M^{-1} s^{-1}]	ref
$[Mn_2(L2)Cl_4]$	47.0 ± 0.2	this work	23.0 ± 0.1	19	19.0 ± 0.1	this work
$[Mn(Me_2\text{-Pyane})]$	27.3 ± 0.1	this work	12.1 ± 0.1	19	5.4 ± 0.6	this work
uncatalyzed	~0.50	56	0.13 ± 0.01	19	0.011 ± 0.001	this work

Scheme 3. Oxidation of O_2^- by a Mn(III)-Peroxo Intermediate and H_2O_2 Release via a Proposed Mechanism in the Literature[57]

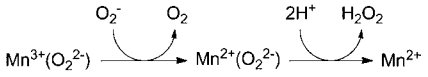

allowed us to detect a stable *trans*-aqua-hydroxo-Mn(II) species in an aqueous solution and to study for the first time the *trans*-effect of the hydroxo group on the water lability of a divalent metal center. The observed labilizing effect of the *trans*-hydroxo ligand is about 100- to 10 000-fold weaker compared to *trans*-M(III)(OH)(H_2O).[20,21] Furthermore, this suggest manipulation of the electronic properties of polydentate ligands could be used to bring pK_a values of coordinated aqua ligands closer to physiological pH (6.5−7.8). Such complexes can provide a platform for the development of MRI contrast agents for *in vivo* applications.[60] In addition, manganese complexes with a terminal aqua ligand play an important role in a number of catalytic biorelevant processes, in particular those involving the activation of small molecules.[61] Thus, manganese species with a hydroxo ligand *trans* to a labile aqua ligand are valuable models for studying the effect of the hydroxo ligand on the activation of small molecules by manganese centers. Performing such types of studies we have observed that the SOD activity per Mn center at pH 10.0 is about 1.8-fold higher in the case of our dinuclear amine complex $[Mn_2(L2)(OH)_2(H_2O)_2]^{2+}$ than in the case of the corresponding mononuclear complex $[Mn(Me_2\text{-Pyane})]$ that is not able to form stable hydroxo species.

In conclusion, even if there is no significant electronic communication between the two manganese(II) centers within the dinuclear complexes $[Mn_2(L1)Cl_4]$ and $[Mn_2(L2)Cl_4]$, such structural framework affects the stability of *trans*-aqua-hydroxo species and consequently solution behavior of the complexes, which can influence their catalytic SOD activity especially at higher pH values. This study establishes baseline speciation and water exchange in noncoordinating aqueous buffer, useful for comparing to the situation under physiological conditions where there is a high concentration of chloride and phosphates, which can affect complex speciation, acidity of any aqua ligand and possibly their SOD activity.

■ ASSOCIATED CONTENT

Supporting Information

Available are crystallographic data. ^{17}O NMR data and data treatment, stopped-flow data, electrochemical data, and mass spectra of relevant compounds. This material is available free of charge via the Internet at http://pubs.acs.org.

■ AUTHOR INFORMATION

Corresponding Author

*E-mail: ivana.ivanovic@chemie.uni-erlangen.de. Fax: +49 9131 8527345. Phone: +49 9131 8525428.

Notes

The authors declare no competing financial interest.

■ ACKNOWLEDGMENTS

Financial support by the DFG (SFB 583) and the intramural grant from University Erlangen-Nürnberg (Emerging Field Initiative: Medicinal Redox Inorganic Chemistry) is gratefully acknowledged. The authors would also gratefully thank Oliver Tröppner and Leanne C. Nye for recording the ESI-mass spectra.

■ REFERENCES

(1) Smith, S. J.; Hadler, K. S.; Schenk, G.; Hanson, G. R.; Mitić, N. *Metals in Biology*; Springer: Berlin, 2010; Vol. *29*.
(2) (a) Riley, D. P. Schall, O. F. *Advances in Inorganic Chemistry*; Elsevier Inc.: Amsterdam, 2007; Vol. *59*. (b) Hicks, S. D.; Petersen, J. L.; Bougher, C. J.; Abu-Omar, M. M. *Angew. Chem., Int. Ed.* **2011**, *50*, 699−702.
(3) De Boer, J. W.; Browne, W. R.; Brinksma, J.; Alsters, P. L.; Hage, R.; Feringa, B. L. *Inorg. Chem.* **2007**, *46*, 6353−6372.
(4) Wang, J.; Slater, B.; Alberola, A.; Stoeckli-Evans, H.; Razavi, F. S.; Pilkington, M. *Inorg. Chem.* **2007**, *46*, 4763−4765.
(5) Kim, K. J.; Park, M.−S.; Kim, J.-H.; Hwang, U.; Lee, N. J.; Jeong, G.; Kim, Y.-J. *Chem. Commun.* **2012**, *48*, 5455−5457.
(6) Aguirre, J. D.; Culotta, V. C. *J. Biol. Chem.* **2012**, *287*, 13541−13548.
(7) Drahoš, B.; Lukeš, I.; Tóth, É. *Eur. J. Inorg. Chem.* **2012**, *12*, 1975−1986.
(8) Pan, D.; Caruthers, S. D.; Senpan, A.; Schmieder, A. H.; Wickline, S. A.; Gregory, M. L. *WIREs Nanomed. Nanobio.* **2011**, *3*, 162−173.
(9) (a) Lu, J.; et al. *Biomaterials* **2009**, *30*, 2919−2928. (b) Bae, K. H.; Lee, K.; Kim, C.; Park, T. G. *Biomaterials* **2011**, *32*, 176−184.
(10) Quintanar, L. *Inorg. Chim. Acta* **2008**, *361*, 875−884.
(11) (a) McConnell, I. L.; Grigoryants, V. M.; Scholes, C. P.; Myers, W. K.; Chen, P.-Y. C.; Whittaker, J. W.; Brudvig, G. W. *J. Am. Chem. Soc.* **2012**, *134*, 1504−1512. (b) Poulsen, A. K.; Rompel, A.; McKenzie, C. J. *Angew. Chem., Int. Ed.* **2005**, *44*, 6916−6920.
(12) Ivanović-Burmazović, I. *Advances in Inorganic Chemistry*; Elsevier Inc.: San Diego, 2008; Vol. *60*.
(13) Ivanović-Burmazović, I.; van Eldik, R. *J. Chem. Soc., Dalton Trans.* **2008**, 5259−5275.
(14) Laurent, S.; Henoumont, C.; Vander Elst, L.; Muller, R. N. *Eur. J. Inorg. Chem.* **2012**, *12*, 1889−1915.
(15) Batinić-Haberle, I.; Rebouças, J. S.; Spasojević, I. *Antioxid. Redox Signaling* **2010**, *13*, 877−918.
(16) Kelso, G. F.; Maroz, A.; Cochemé, H. M.; Logan, A.; Prime, T. A.; Peskin, A. V.; Winterbourn, C. C.; James, A. M.; Ross, M. F.; Brooker, S.; Porteous, C. M.; Anderson, R. F.; Murphy, M. P.; Smith, R. A. J. *Chem. Biol.* **2012**, *19*, 1237−1246.
(17) Balogh, E.; He, Z.; Hsieh, W.; Liu, S.; Tóth, E. *Inorg. Chem.* **2007**, *46*, 238−250.
(18) Caravan, P.; Zhang, Z. *Eur. J. Inorg. Chem.* **2012**, *12*, 1916−1923.
(19) Friedel, F. C.; Lieb, D.; Ivanović-Burmazović, I. *J. Inorg. Biochem.* **2012**, *109*, 26−32.
(20) (a) Kowall, T.; Caravan, P.; Bourgeois, H.; Helm, L.; Rotzinger, F. P.; Merbach, A. E. *J. Am. Chem. Soc.* **1998**, *120*, 6569−6577. (b) Nordin, J. P.; Sullivan, D. J.; Phillips, B. L.; Casey, W. H. *Inorg. Chem.* **1998**, *37*, 4760−4763.
(21) Laurenczy, G.; Rapaport, I.; Zbinden, D.; Merbach, A. E. *Magn. Reson. Chem.* **1991**, *29*, 45−51.

(22) Meier, U. C.; Scopelltiti, R.; Solari, E.; Merbach, A. E. *Inorg. Chem.* **2000**, *39*, 3816−3822.
(23) Baes, C. F., Jr.; Mesmer, R. E. *The Hydrolysis of Cations*; Wiley: New York, 1976.
(24) (a) Drljaca, A.; Zahl, A.; van Eldik, R. *Inorg. Chem.* **1998**, *37*, 3948−3953. (b) Coe, B. J.; Glenwright, S. J. *Coord. Chem. Rev.* **2000**, *203*, 5−80. (c) Houston, J. R.; Yu, P.; Casey, W. H. *Inorg. Chem.* **2005**, *44*, 5176−5182.
(25) Dees, A.; Zahl, A.; Puchta, R.; van Eikema Hommes, N. J. R.; Heinemann, F. W.; Ivanović-Burmazović, I. *Inorg. Chem.* **2007**, *46*, 2459−2470.
(26) (a) Riley, D. P.; Henke, S. L.; Lennon, P. J.; Weiss, R. H.; Neumann, W. L.; Rivers, W. J., Jr.; Aston, K. W.; Sample, K. R.; Rahman, H.; Ling, C.-S.; Shieh, J.-J.; Busch, D. H.; Szulbinski, W. *Inorg. Chem.* **1996**, *35*, 5213−5231. (b) Riley, D. P.; Henke, S. L.; Lennon, P. J.; Aston, K. *Inorg. Chem.* **1999**, *38*, 1908−1917.
(27) Bill, E. *JulX version 1.5, MPI for Bioinorganic Chemistry*; Mülheim an der Ruhr, Germany, 2008.
(28) (a) Fontana, F.; Minisci, F.; Barbosa, M. C. N.; Vismara, E. *J. Org. Chem.* **1991**, *56*, 2866−2869. (b) Zong, R.; Zhou, H.; Thummel, R. P. *J. Org. Chem.* **2008**, *73*, 4334−4337.
(29) Aston, K. W.; Rath, N.; Naik, A.; Slomczynska, U.; Schall, O. F.; Riley, D. P. *Inorg. Chem.* **2001**, *40*, 1779−1789.
(30) (a) Gran, G. *Analyst* **1952**, *77*, 661−671. (b) Gran, G. *Anal. Chim. Acta* **1988**, *206*, 111−123. (c) Martell, A. E.; Motekaitis, R. J. *Determination and Use of Stability Constants*; VCH: Weinheim, Germany, 1992.
(31) Zuberbühler, A. D.; Kaden, T. A. *Talanta* **1982**, *29*, 201−206.
(32) Kitamura, Y.; Itoh, T. *J. Solution Chem.* **1987**, *16*, 715−725; *J. Phys. Chem. Ref. Data* **2002**, *31*, 231−370.
(33) Zahl, A.; Neubrand, A.; Aygen, S.; van Eldik, R. *Rev. Sci. Instrum.* **1994**, *65*, 882−886.
(34) Duerr, K.; Macpherson, B. P.; Warratz, R.; Hampel, F.; Tuczek, F.; Jux, N.; Ivanović-Burmazović, I. *J. Am. Chem. Soc.* **2007**, *129*, 4217−4228.
(35) (a) Barbaro, P.; Bianchini, C.; Giambastiani, G.; Rios, I. G.; Meli, A.; Oberhauser, W.; Segarra, A. M.; Sorace, L.; Toti, A. *Organometallics* **2007**, *26*, 4639−4651. (b) Citterio, A.; Arnoldi, A.; Macerì, C. *Chim. Ind.* **1978**, *60*, 14−15.
(36) Brooker, S.; McKee, V. *J. Chem. Soc., Dalton Trans.* **1990**, 2397−2401.
(37) Omar, J.-S.; Daniel, R.-R.; del María, J. R.-H.; Martha, E. S.-T.; Rafael, Z.-U. *J. Chem. Soc., Dalton Trans.* **1998**, *10*, 1551−1556.
(38) Liu, G.-F.; Filipović, M.; Heinemann, F. W.; Ivanović-Burmazović, I. *Inorg. Chem.* **2007**, *46*, 8825−8835.
(39) Drahoš, B.; Kotek, J.; Hermann, P.; Lukeš, I.; Tóth, E. *Inorg. Chem.* **2010**, *49*, 3224−3238.
(40) Kahn, O. *Molecular Magnetism*; VCH: New York, 1993.
(41) Jackels, S. C.; Durham, M. M.; Newton, J. E.; Henninger, T. C. *Inorg. Chem.* **1992**, *31*, 234−239.
(42) (a) McQuade, L. E.; Pluth, M. D.; Lippard, S. J. *Inorg. Chem.* **2010**, *49*, 8025−8033. (b) Huang, J.; Xu, Y.; Qian, X. *Org. Biomol. Chem.* **2009**, *7*, 1299−1303.
(43) Swift, T. J.; Connick, R. E. *J. Chem. Phys.* **1962**, *37*, 307−320.
(44) Maigut, J.; Meier, R.; Zahl, A.; van Eldik, R. *Inorg. Chem.* **2008**, *47*, 5702−5719.
(45) Schneppensieper, T.; Zahl, A.; van Eldik, R. *Angew. Chem., Int. Ed.* **2001**, *40*, 1678−1680.
(46) Cusanelli, A.; Frey, U.; Richens, D. T.; Merbach, A. E. *J. Am. Chem. Soc.* **1996**, *118*, 5265−5271.
(47) Helm, L.; Mehrbach, A. E. *Chem. Rev.* **2005**, *105*, 1923−1959.
(48) Lieb, D.; Zahl, A.; Shubina, T. E.; Ivanović-Burmazović, I. *J. Am. Chem. Soc.* **2010**, *132*, 7282−7284.
(49) Van Eldik, R. *Inorganic High Pressure*; Elsevier Inc.: Amsterdam, 1986.
(50) Drahoš, B.; Kotek, J.; Císařová, I.; Hermann, P.; Helm, L.; Lukeš, I.; Tóth, É. *Inorg. Chem.* **2011**, *50*, 12785−12801.
(51) Maigut, J.; Meier, R.; Zahl, A.; van Eldik, R. *J. Am. Chem. Soc.* **2008**, *130*, 14556−14569.
(52) Ducommun, Y.; Newman, K. E.; Merbach, A. E. *Inorg. Chem.* **1980**, *196*, 344−349.
(53) An electrochemical−chemical mechanism describes a mechanism where the product of the first redox event evolves chemically. For further literature see: Bard, A. J.; Faulken, L. R. *Electrochemical Methods, Fundamentals and Applications*; Wiley: New York, 2001.
(54) Ghachtouli, S. E.; Guillot, R.; Dorlet, P.; Anxolabéhère-Mallart, E.; Aukauloo, A. *Dalton Trans.* **2012**, *41*, 1675−1677.
(55) Riley, D. P.; Weiss, R. H. *J. Am. Chem. Soc.* **1994**, *116*, 387−388.
(56) Riley, D. P.; Rivers, I. W. J.; Weiss, R. H. *Anal. Biochem.* **1991**, *196*, 344−349.
(57) Maroz, A.; Kelso, G. F.; Smith, R. A. J.; Ware, D. C.; Anderson, R. F. *J. Phys. Chem. A* **2008**, *112*, 4929−4935.
(58) Carrasco, R.; Morgenstern-Badarau, I.; Cano, J. *Inorg. Chim. Acta* **2007**, *360*, 91−101.
(59) Sarauli, D.; van Eldik, R.; Ivanović-Burmazović, I. *BioInorg. React. Mech.* **2012**, *8*, DOI: 10.1515/irm-2012-0008.
(60) Jasanoff, A. *Curr. Opin. Neurobiol.* **2007**, *17*, 593−600.
(61) (a) Gupta, R.; Borovik, A. S. *J. Am. Chem. Soc.* **2003**, *125*, 13234−13242. (b) Galstyan, A.; Robertazzi, A.; Knapp, E. W. *J. Am. Chem. Soc.* **2012**, *134*, 7442−7449.